Numerical study of the stability of the Interior Penalty Discontinuous Galerkin method for the wave equation with 2D triangulations

Cyril Agut, Jean-Michel Bart, Julien Diaz

INRIA

INSTITUT NATIONAL DE RECHERCHE EN INFORMATIQUE ET EN AUTOMATIQUE

Numerical study of the stability of the Interior Penalty Discontinuous Galerkin method for the wave equation with 2D triangulations

Cyril Agut — Jean-Michel Bart — Julien Diaz

N° 7719

Aout 2011

Observation and Modeling for Environmental Sciences

ISSN 0249-6399 ISRN INRIA/RR--7719--FR+ENG

INSTITUT NATIONAL
DE RECHERCHE
EN INFORMATIQUE
ET EN AUTOMATIQUE

INRIA

centre de recherche
BORDEAUX - SUD OUEST

Numerical study of the stability of the Interior Penalty Discontinuous Galerkin method for the wave equation with 2D triangulations

Cyril Agut*†, Jean-Michel Bart† ‡ , Julien Diaz† *

Theme : Observation and Modeling for Environmental Sciences
Équipe-Projet Magique-3d

Rapport de recherche n° 7719 — Aout 2011 — 45 pages

Abstract: We are interesting in the well known Interior Penalty Discontinuous Galerkin method applied to the acoutic wave equation. More precisely, we propose a numerical study to determine the most suitable choice for the coefficient of penalization involved in the method. In [1], we have explained anlytically how to choose, in the one dimensional case, this coefficient and we have proposed an extension to squared meshes in 2D and cubic meshes in 3D. Herein, the purpose of this work is to determine numerically the best choice of this coefficient for triangular 2D meshes and the consequences over the CFL condition.

Key-words: Discontinuous Galerkin, penalization coefficient, CFL condition, wave equation

* LMAP - University of Pau
† INRIA Project-Team Magique-3D
‡ INSA Toulouse, third year engineer student

Centre de recherche INRIA Bordeaux – Sud Ouest
Domaine Universitaire - 351, cours de la Libération 33405 Talence Cedex
Téléphone : +33 5 40 00 69 00

Etude numérique de la stabilité de la méthode de Galerkine Discontinue avec Pénalité Intérieure pour l'équation des ondes avec une traingulation 2D.

Résumé : Nous nous intéressons ici à la méthode de Galerkine Discontinue avec Pénalité Intérieure appliquée à l'équation des ondes acoustiques. Plus précisément, nous proposons une étude numérique afin de déterminer le choix le plus judicieux du coefficient de pénalisation intervenant dans cette méthode. Dans [1], nous avons établi analytiquement comment choisir de manière optimale ce coefficient en 1D puis nous avons proposé une extension à des maillages quadrangulaires réguliers en 2D ou cubiques en 3D. Le but de cette nouvelle étude est de caractériser numériquement ce dernier dans le cas de maillage triangulaire 2D ainsi que ses conséquences sur la condition CFL du schéma.

Mots-clés : Galerkine Disconitnue, coefficient de pénalisation, condition CFL, équation des ondes

1 Introduction

This research report can be seen as the second part of [1] in which we have proposed an analytical study of the stability of the Interior Penalty Discontinuous Galerkin (IPDG) (cf. [4, 5, 6, 2]) method for the wave equation in the case of cartesian grids (segments in 1D, squares in 2D and cubes in 3D). The IPDG method is a particular Discontinuous Galerkin Method (DGM) and therefore, when we focus on transient problems, the mass matrix we have to invert is easily invertible, since it is block diagonal by construction, which leads to quasi explicit schemes. Moreover, we can easily take into account the variations of the physical parameters thanks to the discontinuities of the basis functions we consider and these methods have also very good properties for parallel computing since all the volume integrals are computed locally and the communications between the cells are ensured by integrals over the faces of the elements. Finally, among all the DGM, the IPDG method is known to be stable and consistent (cf. [3]) but unfortunately suffers from two difficulties.
The first one is the determination of the penalization parameter, which penalizes the discontinuities of the solution through the faces. The accurate determination of the optimal parameter is crucial, since a too small value leads to instabilities while a too large value could (strongly) hamper the CFL (Courant-Friedrichs-Lewy) condition, which gives the maximal time step that can be used to ensure the stability of the scheme. The second difficulty is the determination of the CFL condition and it is well-known that this condition decreases when the penalization parameter increases.
These difficulties have to be overcome to take fully advantage of the IPDG method. Therefore in [1], we have explicited the optimal choice of the coefficient of penalization and its influence over the CFL condition of the scheme on cartesian grids. We have proved in an original way and extended the well known conjecture proposed in [2] by Ainsworth, Monk and Muniz. We have also derived results over the penalization coefficient with squared meshes in 2D and cubic meshes in 3D. Nevertheless, since the parameter of penalization depends strongly on the geometrical shape of the mesh, these results should be extended to more general meshes. We also considered the case of rectangular and parallelepipedic cells in [1], but it is still a too particular case. Consequently, in this work we propose a numerical study to explicit the choice of a good coefficient of penalization in the case of triangular 2D meshes.
In section 2, we recall the system obtained thanks to an IPDG method and in section 3, we briefly present the results obtained in [1] that we want to extend to the case of triangular cells. Section 4 illustrates that the inscribed circle of the cells has an important influence on the penalization parameter. Finally, in section 5, we show that taking into account the inscribed circle and the angles of the cells leads to a very accurate definition of the penalization parameter.

2 Discretization of the acoustic wave equation

In this section, we present the so called Interior Penalty Discontinuous Galerkin method applied to the acoustic wave equation in homogeneous bounded media $\Omega \subset \mathbb{R}^d, d = 1, 2, 3$. For the sake of simplicity, we impose homogeneous Neumann boundary conditions on the boundary $\Gamma := \partial\Omega$ but this study can be extended

to Dirichlet boundary conditions without major difficulties.

$$\begin{cases} \text{Find } u : \Omega \times [0,T] \mapsto \mathbb{R} \text{ such that :} & \\ \dfrac{1}{\mu}\dfrac{\partial^2 u}{\partial t^2} - \operatorname{div}\left(\dfrac{1}{\rho}\nabla u\right) = f & \text{in } \Omega \times]0,T], \\ u(x,0) = u_0, \quad \dfrac{\partial u}{\partial t}(x,0) = u_1 & \text{in } \Omega, \\ u = 0 & \text{on } \partial\Omega. \end{cases} \tag{1}$$

where u stands for the displacement, μ is the compressibility modulus, ρ is the density and f is the source term.
We introduce a triangulation $\mathcal{T}_h$ of Ω and the following space of approximation with piecewise discontinuous polynomial functions :

$$V_h := \left\{ v \in L^2(\Omega) \, : \, v_{|K} \in P^p(K), \forall K \in \mathcal{T}_h, p \geq 3 \right\}.$$

The set of the mesh faces are denoted $\mathcal{F}_h$ which is partitionned into two subsets $\mathcal{F}_h^i$ and $\mathcal{F}_h^b$ corresponding respectively to the interior faces and those located on the boundary. For $F \in \mathcal{F}_h^i$, we note arbitrarily K^+ and K^- the two elements sharing F and we define ν as the unit outward normal vector pointing from K^+ to K^-. Moreover, $v^\pm$ represents the restriction of a function v to the element $K^\pm$ and we define the jump and the average of a piecewise smooth function $v \in V_h$ over $F \in \mathcal{F}_h^i$ such that:

$$[\![v]\!] = v^+ - v^-, \qquad \{\!\{v\}\!\} = \frac{v^+ + v^-}{2} \tag{2}$$

and for $F \in \mathcal{F}_h^b$ such that $[\![v]\!] = v$ and $\{\!\{v\}\!\} = v$.
The IPDG discretization of (1) reads as

$$\begin{cases} \text{Find } u_h \in V_h \text{ such that,} \quad \forall v_h \in V_h : & \\ \displaystyle\sum_{K \in \mathcal{T}_h} \int_K \frac{1}{\mu} \partial_t^2 u_h v_h \, dx = & -a_h(u_h, v_h) + \displaystyle\sum_{K \in \mathcal{T}_h} \int_K f v_h \, dx. \end{cases} \tag{3}$$

where a_h is a bilinear form defined by

$$a_h(u_h, v_h) = B_{\mathcal{T}_h}(u_h, v_h) - \mathcal{I}(u_h, v_h) - \mathcal{I}(v_h, u_h) + B_S(u_h, v_h),$$

with

$$B_{\mathcal{T}_h}(u_h, v) = \sum_{K \in \mathcal{T}_h} \int_K \frac{1}{\rho} \nabla u_h \nabla v, \quad \mathcal{I}(u_h, v) = \sum_{F \in \mathcal{F}_h^i} \int_F [\![v]\!] \left\{\!\!\left\{ \frac{1}{\rho} \nabla u_h \cdot \boldsymbol{\nu} \right\}\!\!\right\},$$

$$B_S(u_h, v) = \sum_{F \in \mathcal{F}_h^i} \int_F \gamma [\![u_h]\!] [\![v]\!].$$

The bilinear form B_S is devoted to enforce the coercivity of a_h and the penalization function γ is defined on each interior face F by

$$\gamma = \frac{\alpha}{\xi_F}$$

where α is a positive parameter. There are many definitions of the function ξ_F in the litterature. The most commonly used are:

- $\xi_F = h(F)$ where $h(F)$ denotes the diameter F. See for instance [3, 2, 6]. It is worth noting that that this definition does not make sense in 1D.
- $\xi_F = \min(h(K^+), h(K^-))$ where $h(K^\pm)$ is the diameter of $K^\pm$. See for instance [5].
- $\xi_F = \min(\rho_{K^+}, \rho_{K^-})$ where $\rho(K^\pm)$ is the diameter of the inscribed circle (or sphere) of $K^\pm$. See for instance [7].

Whatever the definition of ξ_F, the coercivity of a_h is ensured for $\alpha \geq \alpha_0$. Obviously, the optimal parameter α_0 depends on the choice of the basis functions of V_h, but also on ξ_F. It has been shown by Shabazi in [7] that the third definition was the most appropriate for triangular meshes.
At this point, we choose not to explicit the expression of ξ_F. This will be done in the next section.
We refer to [3, 2, 5] for more details on the properties of the bilinear form a_h.

Considering $\{\varphi_i\}_{i=1,\dots,m}$ the classical discontinuous Lagrange basis functions of degree p of V_h, where m denotes the number of degrees of freedom of the problem, we obtain the following linear system:

$$\partial_t^2 U = M^{-1}KU + M^{-1}F \tag{4}$$

where

$$(M)_{i,j} = \sum_{K\in\mathcal{T}_h} \int_K \varphi_i\varphi_j,\ (K)_{i,j} = a_h(\varphi_i,\varphi_j),\ (F)_i = \sum_{K\in\mathcal{T}_h} \int_K f\varphi_i.$$

Now, we have to discretize in time. Using the well known Leap-Frog scheme, we obtain the following fully discretized scheme:

$$\frac{U^{n+1} - 2U^n + U^{n-1}}{\Delta t^2} = -M^{-1}KU^n + M^{-1}F^n. \tag{5}$$

3 Stability analysis

In this section, we recall the main results wa have obtained in [1]. First we have proposed necessary conditions over γ and Δt ensuring the L^2- stability of scheme (5). This theorem provides an explicit dependence of Δt with respect to γ and h. Next we have proposed a sufficient and necessary stability condition. In this second theorem, the dependence of Δt with respect to γ is no longer explicit. However the CFL condition can be numerically computed using the roots of a polynomial of degree $2p$. We assume here that the domain Ω is unbounded $(\Omega = \mathbb{R}^d)$ and uniformly meshed by segments (if $d = 1$), squares (if $d = 2$) or cubes (if $d = 3$). The length of the edges of the elements is denoted by h.

The necessary stability conditions are given by the following theorem.

Theorem 3.1. *The scheme (5) is L^2-stable only if, for $p \leq 5$,*

$$\gamma \geq \frac{p(p+1)}{2h}; \tag{6}$$

and, denoting $\alpha = \gamma/h$,

$$\sqrt{d}\frac{c\Delta t}{h} \leq \begin{cases} C_{1,p} & \text{if } \alpha \leq \alpha_{1,p} \\ C_{2,p}(\alpha) & \text{if } \alpha > \alpha_{1,p}. \end{cases} \tag{7}$$

where $\alpha_{1,p}$, $C_{1,p}$ *and* $C_{2,p}(\alpha)$ *are defined with respect to the polynomial degree* p *such that:*

p	$\alpha_{1,p}$	$C_{1,p}$
1	2	$\frac{\sqrt{3}}{3} \simeq 0.577$
2	$\frac{27}{5} = 5.4$	$\frac{1}{\sqrt{15}} \simeq 0.258$
3	$\frac{2\sqrt{1605}+393}{49} \simeq 9.65$	$\sqrt{\frac{2}{45+\sqrt{1605}}} \simeq 0.153$
4	$\alpha_{1,4} \simeq 14.7$	$\sqrt{\frac{2}{3\left(35+\sqrt{805}\right)}} \simeq 0.103$
5	$\alpha_{1,5} \simeq 20.8$	$\sqrt{\frac{1}{10\sqrt{133}\cos(g_5)+70}} \simeq 0.074$

and

p	$C_{2,p}(\alpha)$
1	$\frac{1}{\sqrt{3(\alpha-1)}}$
2	$\sqrt{\frac{2}{-15+6\alpha+\left(405-240\alpha+36\alpha^2\right)^{1/2}}}$
3	$\sqrt{\frac{2}{-45+10\alpha+\left(4545-1320\alpha+100\alpha^2\right)^{1/2}}}$
4	$\sqrt{\frac{1}{2\sqrt{5}g_{4,1}(\alpha)\,g_{4,2}(\alpha)+5\alpha-35}}$
5	$\sqrt{\frac{1}{2\sqrt{7}g_{5,1}(\alpha)\,g_{5,2}(\alpha)+7(\alpha-10)}}$

where, for the case $p = 4$, *we have*

$$\begin{cases} g_{4,1}(\alpha) = & \left(518-98\alpha+5\alpha^2\right)^{\frac{1}{2}}, \\ g_{4,2}(\alpha) = & \cos\left(\frac{1}{3}\arccos\left(\frac{1}{10}g_{4,3}(\alpha)\frac{\sqrt{5}}{g_{4,1}^3(\alpha)}\right)\right), \\ g_{4,3}(\alpha) = & -47705+14574\alpha-1470\alpha^2+50\alpha^3 \end{cases}$$

and for the polynomials of degree 5,

$$\begin{cases} g_5 = & \frac{1}{3}\arccos\left(\frac{10447}{126350}\sqrt{133}\right) \\ g_{5,1}(\alpha) = & \left(1555 - 200\alpha + 7\alpha^2\right)^{\frac{1}{2}}, \\ g_{5,2}(\alpha) = & \cos\left(\frac{1}{3}\arccos\left(\frac{1}{14}g_{5,3}(\alpha)\frac{\sqrt{7}}{g_{5,1}^3(\alpha)}\right)\right), \\ g_{5,3}(\alpha) = & -299825 + 61440\alpha - 4200\alpha^2 + 98\alpha^3. \end{cases}$$

Remark 3.2.

- *As it is was noted in [6], the stability condition on Δt behaves as $C/\sqrt{\alpha}$ for large α. More precisely, $C = \sqrt{\frac{2}{(p+1)(p+2)}}$.*
- *This stability condition is constant for $\frac{p(p+1)}{2} \leq \alpha \leq \alpha_p^1$. This shows that it is not necessary to choose α too close from α_0 to improve the CFL condition.*

However, the above condition is only necessary. To obtain the actual CFL, we need the following necessary and sufficient condition.

Theorem 3.3. *The scheme (5) is L^2-stable if and only if, for $p \leq 5$, (6) and (7) are satisfied and*

$$\sqrt{d}\frac{c\Delta t}{h} \leq C_{3,p}(\alpha) \tag{8}$$

where $C_{3,p}(\alpha) = min\left\{\lambda \in \mathbb{R} : Q_{p,\alpha}(\lambda) = 0 \text{ and } |\tilde{Q}_{p,\alpha}(\lambda)| \leq 1\right\}$ where $Q_{p,\alpha}(\lambda)$ is a polynomial of degree $2p$ and $\tilde{Q}_{p,\alpha}(\lambda)$ is a rational function. We give in appendix B the expressions of these two functions for $1 \leq p \leq 5$.

Remark 3.4.

- *This theorem does not provide an explicit CFL condition. However it can be computed numerically by the following algorithm:*
  1. *Compute all the roots of $Q_{p,\alpha}$,*
  2. *Select the real roots such that $|\tilde{Q}_{p,\alpha}(\lambda)| \leq 1$,*
  3. *Choose the minimum.*
- *The numerical study of condition (8) shows that the set V_α is actually empty except when α belongs to a small segment around α_1^p. This means that theorem 3.1 provides a sufficient and necessary stability condition when α is not in this segment. Moreover the remarks 3.2 are still valid.*
- *In [2], they authors proved (6) for $p = 0, \ldots, 3$ and conjectured this relation for any p. Theorem (3.3) extends its validity until $p = 5$.*
- *The condition (6) does not depend on the dimension d. This would not have been the case if we had expressed γ as a function of the circumcircle (or circumsphere) diameter which is $\sqrt{d}h$. Since h is the diameter of the inscribed circle or sphere, we conjecture that the third definition of ξ_F is the most appropriate. We will strengthen when we discuss the extension of this theorem to meshes composed of rectangles or parallelepipeds.*

We were unfortunately unable to establish this theorem for any p neverthless the proof for $p \leq 5$ is presented in [1] but also its extension to $d = 2$ (squared meshes) and $d = 3$ (cubic meshes).

For the sake of simplicity, we have restricted our theorem to the case of squared or cubic mesh. However, one can extend the proof to the case of rectangular or parallelepipeds meshes to show that a necessary stability condition is in 2D:

$$\alpha \geq \frac{p\,(p+1)}{2\min\,(h_x, h_y)}$$

and in 3D:

$$\alpha \geq \frac{p\,(p+1)}{2\min\,(h_x, h_y, h_z)}.$$

Here, h_x, h_y and h_z denote respectively the length of the edges of the elements in the x, y and z direction. The minimal value of h_x, h_y and h_z is actually the diameter of the inscribed sphere of each element. This remark confirms that the third definition of ξ_F using the diameter of the inscribed sphere or circle in 2D is the most appropriate.

4 Comparison of the various definitions of ξ_F

The remarks of the previous section show that ξ_F should be the diameter of the inscribed circle (in 2D) or inscribed sphere (in 3D). However, the results are only valid for regular meshes with rectangular or parallelepipedic cells. The aim of this work is to extend the analysis to the case of triangular meshes. To determine the most appropriate definition of ξ_F, we propose to consider regular meshes constructed from a reference triangle as follows. Let K_0 be the triangle $A = (0,0)$, $B = (1,0)$, $C = (x_1, y_1)$ (see Fig. 1), with $y_1 > 0$. The

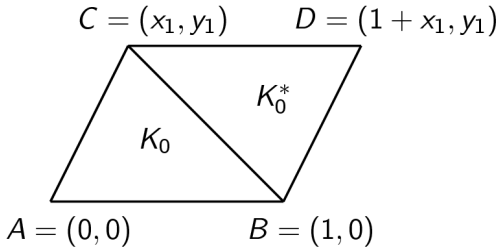

Figure 1: K_0 and K_0^*

coordinate x_1 determine the nature of K_0 : right triangle for $x_1 = 0$, isoscele for $x_1 = 0.5$ and scalene for any other value. We also define K_0^*, the triangle C, B, $D = (1 + x_1, y_1)$. Since $K_0 \cup K_0^*$ is a parallelogram, we easily construct a periodic uniform mesh by translation of $K_0 \cup K_0^*$ along the axis $(1,0)$ and (x_1, y_1) (see Fig. 2). For each kind of reference triangle we wish to compute $\gamma_{\min}$, the minimal value of γ ensuring the stability of the method, and to express it as a function of the geometric characteristic of K_0.

We first considered infinite meshes and, using Fourier transform along the di-

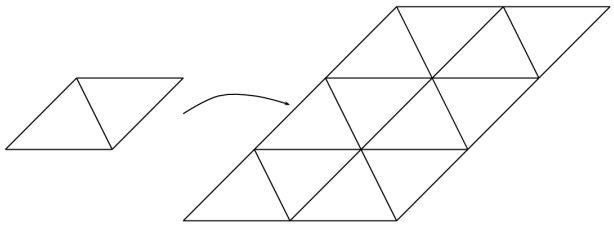

Figure 2: Construction of a periodic mesh

rections $(1,0)$ and (x_1,y_1), we performed a similar analysis to [1]. We did not have particular difficulties to compute the minimal penalization parameter for a given point (x_1,y_1) with P^1 basis functions. However, we did not succeed in expressing this parameter as a function of (x_1,y_1) or of any geometrical characteristic of K_0 and we could not compute it for P^2 and P^3 basis functions. We give in appendix A the details of the computation for right and isoscele triangles.
Then, we decided to compute $\gamma_{\min}$ numerically instead of computing its analytical expression. We considered finite meshes composed of thirty triangles in both directions $(1,0)$ and (x_1,y_1). The expression of the source term in time is given by

$$f(t) = 2\lambda\left(\lambda\left(t-t_0\right)^2 - 1\right)e^{-\lambda(t-t_0)^2},$$

with $x_0 = (0, 0.5)$, $\lambda = \pi^2 f_0^2$, $f_0 = 5$ and $t_0 = 1/f_0$.
The minimal parameter, defined as the smallest parameter ensuring the stability of the IPDG scheme, was computed by dichotomy using algorithm 1. The principle of this algorithm consists in solving the wave equation for a given parameter and then in decreasing this parameter if the scheme is stable or in increasing it else.

Algorithm 1

1: $\Delta t = 4.3E-4$, $\gamma_1 = 1$ and $\gamma_2 = 5$
2: $\gamma = \dfrac{\gamma_1+\gamma_2}{2}$
3: We compute the solution of (1) with Δt and γ after 10000 iterations
4: **if** explosion **then**
5: $\quad \gamma_1 = \gamma$
6: **else**
7: $\quad \gamma_2 = \gamma$
8: **end if**
9: **if** $|\gamma - \dfrac{\gamma_1+\gamma_2}{2}| < 10^{-5}$ **then**
10: $\quad \gamma_{\min} = \gamma_2$
11: **else**
12: $\quad$ Return in 2.
13: **end if**

To determine whether or not the scheme explodes we computed at each time

step the energy

$$E^{n+\frac{1}{2}} = \left(M \frac{U^{n+1} - U^n}{\Delta t}, \frac{U^{n+1} - U^n}{\Delta t} \right) + \left(KU^n, U^{n+1} \right).$$

If it remained constant during the 10000 iterations, i.e. if $E^{n+\frac{1}{2}}$ is not greater than $10e16$, the scheme was considered stable, otherwise it was considered unstable.
The time step Δt has been chosen small enough so that only the penalization parameter could induce instabilities. Recalling that we expect $\gamma_{\min}$ to be under the form

$$\gamma_{\min} = \frac{\alpha_{\min}}{\xi_F}$$

with $\alpha_{\min}$ independent of the geometry of the mesh, the most appropriate definition of ξ_F should be such that $\gamma_{\min}\xi_F$ is independent of the geometry of the mesh, in particular independent of y_1 and x_1. We first considered three configurations

- configuration 1: K_0 is a right triangle, $x_1 = 0$,
- configuration 2: K_0 is an isoscele triangle, $x_1 = 0.5$,
- configuration 3: K_0 is a scalene triangle, $x_1 = 0.75$

and we computed $\gamma_{\min}$ for various values of y_1 using P^1 elements. In Fig. 3 (resp. 4 and 5), we plot the value of $\gamma_{\min}\rho_{\text{ins}}$ (black line) and $\gamma_{\min}\rho_{\text{circ}}$ (red dashed line) as functions of y_1 for $x_1 = 0$ (resp. $x_1 = 0.5$ and $x_1 = 0.75$). It is clear that $\gamma_{\min}\rho_{\text{circ}}$ depends strongly on y_1 and therefore on the geometry of the reference triangle, while $\gamma_{\min}\rho_{\text{ins}}$ seems to be much more independent of y_1 and x_1. Moreover, $\gamma_{\min}\rho_{\text{circ}}$ goes to infinity when y_1 goes to infinity whereas $\gamma_{\min}\rho_{\text{circ}}$ is bounded.

We obtained similar results for P^2 elements (see Fig. 6-8) and for P^3 elements (see Fig. 9-11). Therefore, we conclude that $\xi_F = \rho_{\text{ins}}$ is a more appropriate definition than $\xi_F = \rho_{\text{circ}}$. However, it is clear in all the figures (especially in Fig. 9-11) that $\gamma_{\min}\rho_{\text{circ}}$ slightly depends on y_1. This means that the definition of ξ_F could be improved taking into account other parameters. It is the aim of the following sections.

5 Improvement of the definition of ξ_F

As we said previously, the product $\gamma_{\min} \times \rho_{\text{ins}}$ is not constant and depends slightly on x_1 and y_1. Since it is difficult to analyze numerically the dependence of one quantity with respect to the two parameters, we tried to find another geometrical parameter, which could better describe the variation of $\gamma_{\min}\rho_{\text{ins}}$. It appeared that the minimum angle of K_0, that we denote by $\theta_{\min}$, was the most appropriate. To illustrate this point, we plot in Fig. 12 $\gamma_{\min}\rho_{\text{ins}}$ as a function of $\theta_{\min}$ for P^1 elements and for $x_1 = 0$ (black line), $x_1 = 0.5$ (dotted red line) and $x_1 = 0.75$ (dashed blue line).
Even if the variation of $\gamma_{\min}\rho_{\text{ins}}$ is not as large as the variation of $\gamma_{\min}\rho_{\text{circ}}$, it is almost 100% (from 0.5 to 1), which is still important.

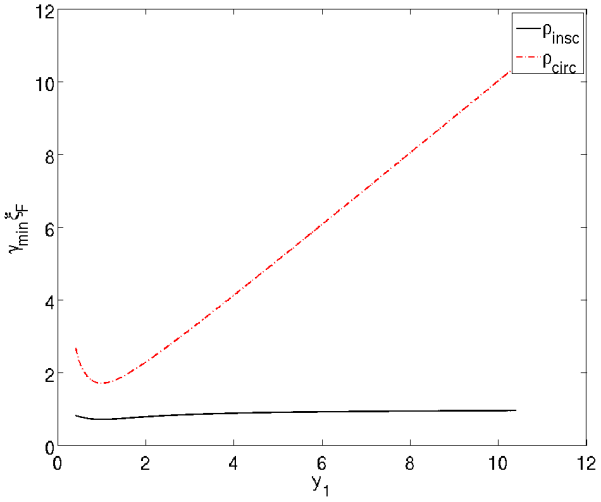

Figure 3: $\gamma_{\min}\xi_F$ for $x_1 = 0$ using P^1 elements

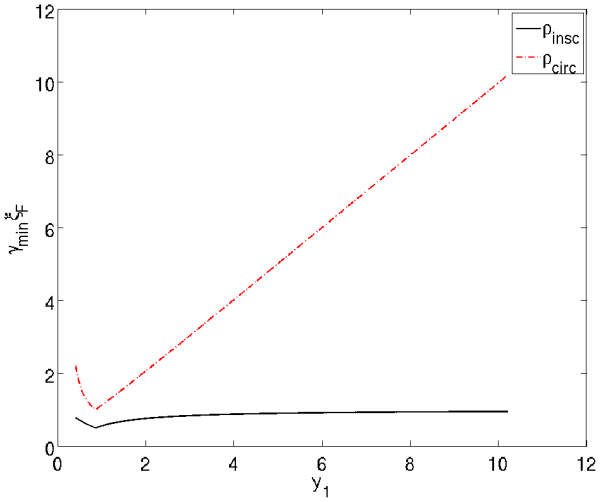

Figure 4: $\gamma_{\min}\xi_F$ for $x_1 = 0.5$ using P^1 elements

Let us remark that each graph is actually composed of two branches (for the right triangle, these two branches are superimposed). In order to explain this phenomenon, we assume, without any loss of generality, that $x_1 \leq 0.5$. This is due to the fact that the minimum angle is the angle $\widehat{ABC}$ (cf. first triangle in figure 13) for small y_1 and the angle $\widehat{ACB}$ for large y_1 (cf. second triangle in figure 13). The critical point, joining the two branches of the curves is obtained when y_1 is such that $\widehat{ACB} = \widehat{ABC}$ (cf. third triangle in figure 13). For the right triangles ($x_1 = 0$), this point corresponds to $y_1 = 1$, i.e. K_0 is a right isoscele triangle.

Let us now focus on the case of isoscele triangles. It is clear that the critical

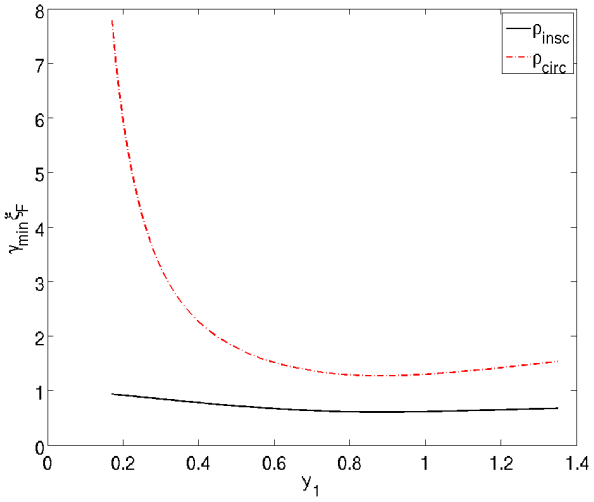

Figure 5: $\gamma_{\min}\xi_F$ for $x_1 = 0.75$ using P^1 elements

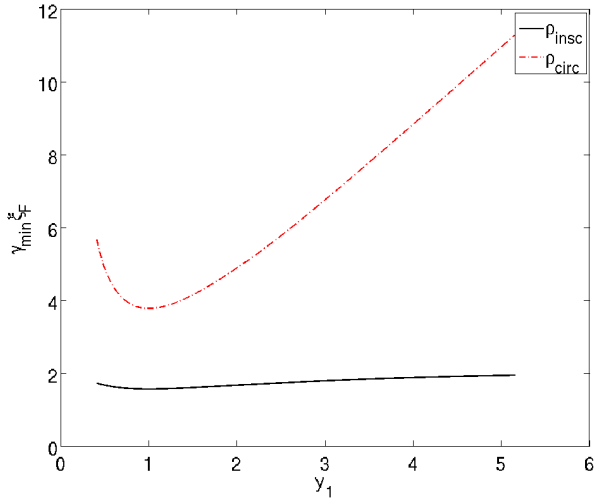

Figure 6: $\gamma_{\min}\xi_F$ for $x_1 = 0$ using P^2 elements

point corresponds to the case where K_0 is equilateral and $y_1 = \dfrac{\sqrt{3}}{2}$. The upper branch is obtained for $y_1 < \dfrac{\sqrt{3}}{2}$, it corresponds to isoscele triangles of base angle smaller that $\dfrac{\pi}{3}$. The lower branch is obtained when $y_1 > \dfrac{\sqrt{3}}{3}$, it corresponds to isoscele triangles of base angle greater that $\dfrac{\pi}{3}$. The upper branch seems to be a maximum of $\gamma_{\min}\xi_F$ while the lower branch seems to be a minimum.

To investigate this point we considered five other configurations which are plotted in Fig. 15.

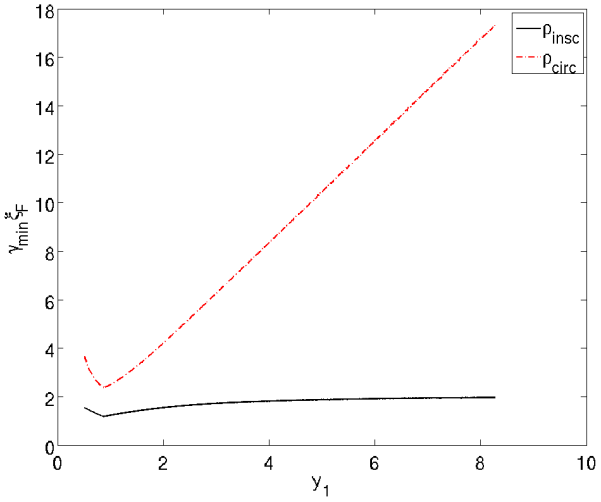

Figure 7: $\gamma_{\min}\xi_F$ for $x_1 = 0.5$ using P^2 elements

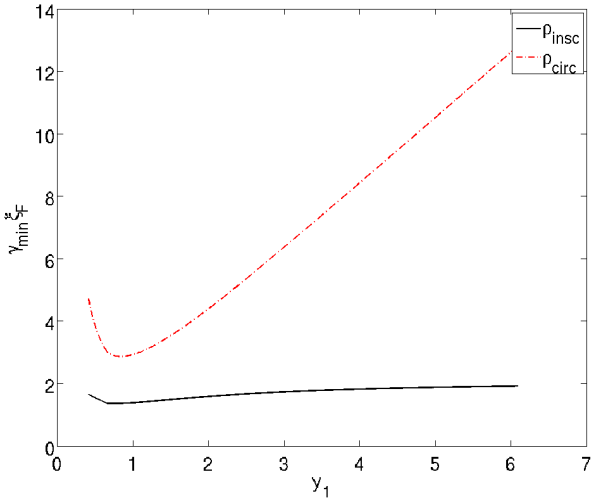

Figure 8: $\gamma_{\min}\xi_F$ for $x_1 = 0.75$ using P^2 elements

- $x_1 = 0.66$ and plotted in blue,
- $x_1 = 0.12$ and plotted in magenta,
- $x_1 = 1.5$ and plotted in dark green,
- $x_1 = 1.3$ and plotted in cyan,
- $x_1 = 1.1$ and plotted in orange.

Note that the three last configurations correspond to obtuse-angled triangles ($x_1 > 1$) so that our analysis is not restricted to sharp-cornered triangles. It is

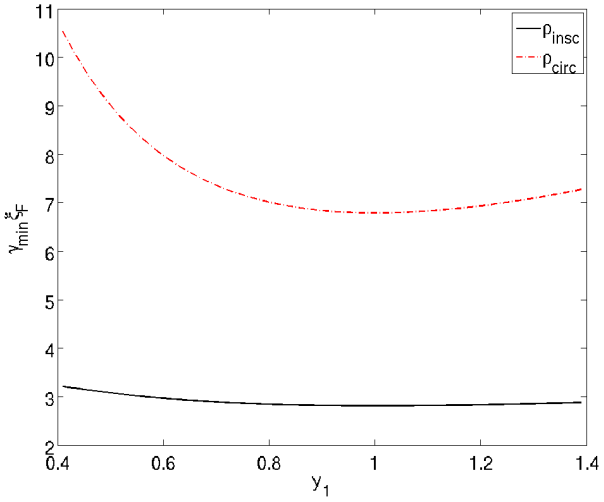

Figure 9: $\gamma_{\min}\xi_F$ for $x_1 = 0$ using P^3 elements

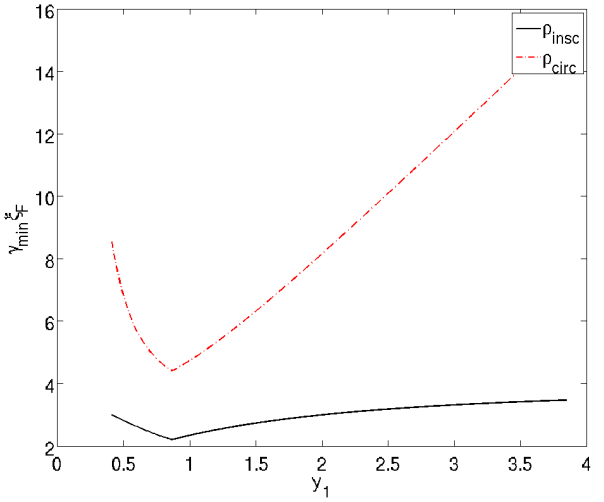

Figure 10: $\gamma_{\min}\xi_F$ for $x_1 = 0.5$ using P^3 elements

clear in Fig. 15 that, whatever the configuration, the upper branch of isoscele triangle is an upper bound of $\gamma_{\min}\rho_{\text{ins}}$ while the lower branch is a lower bound. We performed similar experiments for P^2 (see Fig. 16) and P^3 elements (see Fig. 17) and we obtained the same conclusion.
We are now willing to determine the expression of these two branches as functions of $\theta_{\min}$ to improve the definition of ξ_F. This will be the object of the two next subsections, while the third will be devoted to the study of a third parameter, the maximal angle of the reference triangle.

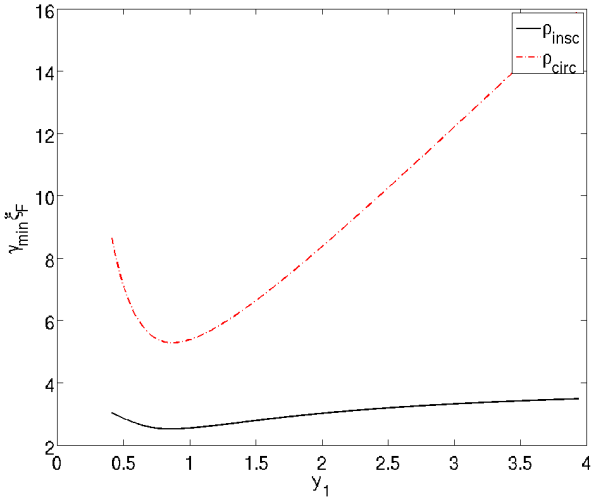

Figure 11: $\gamma_{\min}\xi_F$ for $x_1 = 0.75$ using P^3 elements

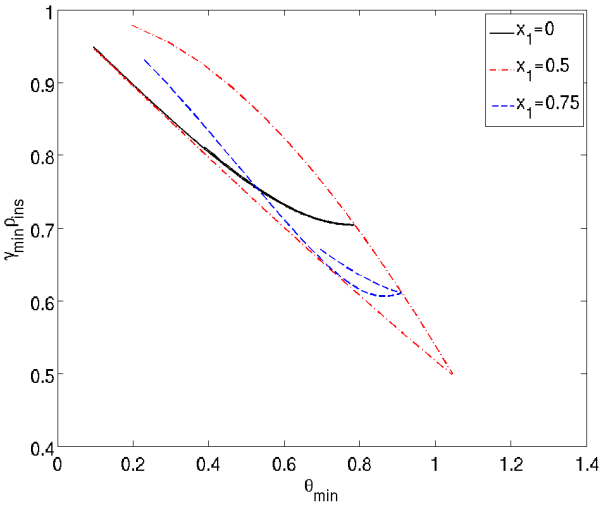

Figure 12: $\gamma_{\min}\rho_{\text{ins}}$ as a function of $\theta_{\min}$ in P^1

5.1 Upper bound of $\gamma_{\min}\rho_{\text{ins}}$

To approximate the upper branch of isoscele triangles we tried various polynomial approximations but trigonometric functions appeared to be more appropriate. Actually, the function

$$f_{1,1} \; : \; \theta_{\min} \longmapsto f_{1,1}\left(\theta_{\min}\right) = \cos\left(\theta_{\min}\right),$$

provides an accurate approximation of this branch. In Fig. 18, we plot f_1 (red line) and the upper branch (black line with +), the curves are superimposed. In Fig. 19, we plot the relative error between the two functions, this error is smaller

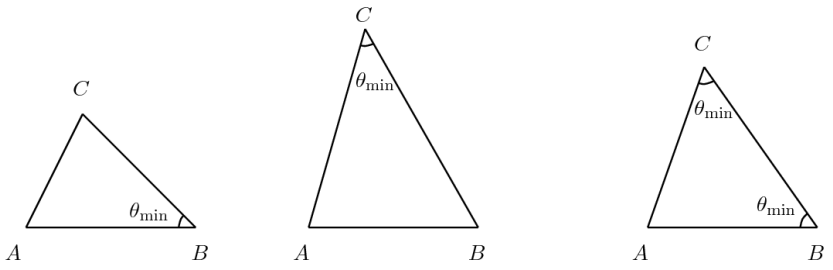

Figure 13: Minimum angle as a function of the nature of the triangle.

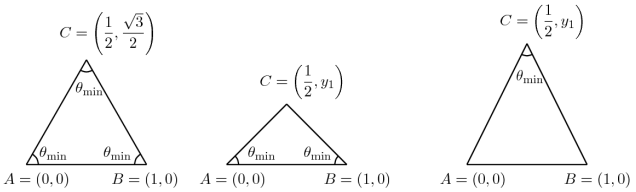

Figure 14: Isoscele triangles for $y_1 = \frac{\sqrt{3}}{2}$, $y_1 < \frac{\sqrt{3}}{2}$ and $y_1 > \frac{\sqrt{3}}{2}$.

than $3\,{}^0/_{00}$. Since $\gamma_{\min}$ is computed numerically with three digits accuracy, f_1 is a very close approximation of $\gamma_{\min}\rho_{\text{ins}}$ for isoscele triangles with $y_1 < \dfrac{\sqrt{3}}{3}$.

f_1 is also an upper bound of $\gamma_{\min}\rho_{\text{ins}}$ for every configurations we considered. Therefore, a better definition of ξ_F should be

$$\xi_F = \frac{\rho_{\text{ins}}}{f_{1,1}}. \tag{9}$$

In Fig. 20, we plot $\dfrac{\gamma_{\min}\rho_{\text{ins}}}{f_{1,1}}$ for the eight configurations we considered. This quantity varies from 0.85 to 1 (18%) and $\dfrac{\rho_{\text{ins}}}{f_{1,1}}$ is then a better definition of ξ_F than ρ_{ins}, which led to variations of 100%.

For P^2 and P^3 polynomials, we found out, using least square method, that a good approximation of the upper branch was respectively

$$f_{1,2} \ : \ \theta_{\min} \longmapsto f_{1,2}\left(\theta_{\min}\right) = 0.13 + 1.85\cos\left(\theta_{\min}\right) + 0.16\sin\left(\theta_{\min}\right),$$

and

$$f_{1,3} =: \ \theta_{\min} \longmapsto f_{1,3}\left(\theta_{\min}\right) = 0.29 + 3.21\cos\left(\theta_{\min}\right) + 0.36\sin\left(\theta_{\min}\right),$$

In Fig. 21 (resp. Fig. 23), we represent $f_{1,2}$ (resp. $f_{1,3}$) and the upper branch for P^2 (resp. P^3) polynomials. Once again, the curves are superimposed. In Fig. 22 (resp. Fig. 24) we plot the relative error between the two functions for P^2 (resp. P^3) polynomials.

In Fig. 25 (resp. Fig. 26) we plot $\dfrac{\gamma_{\min}\rho_{\text{ins}}}{f_{1,2}}$ (resp. $\dfrac{\gamma_{\min}\rho_{\text{ins}}}{f_{1,3}}$) for the eight

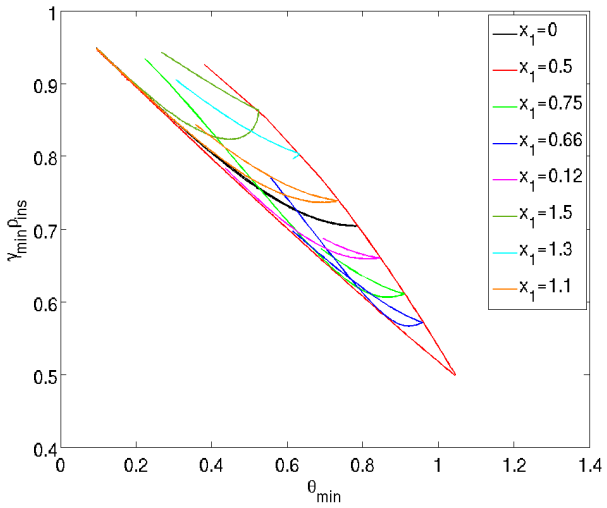

Figure 15: $\xi_F = \rho_{ins}$ for eight configurations in P^1

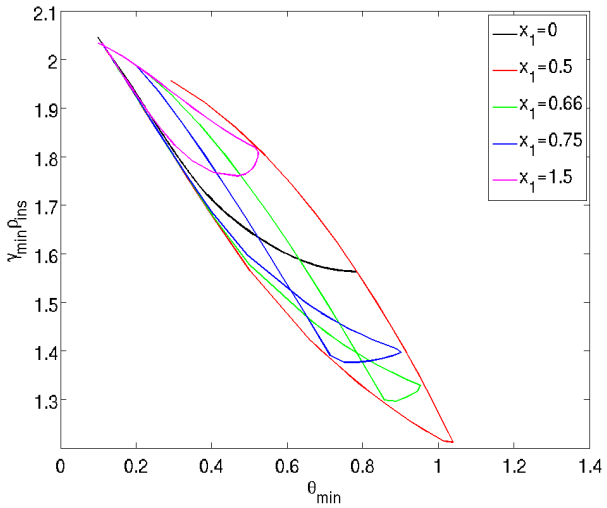

Figure 16: $\xi_F = \rho_{ins}$ for five configurations in P^2

configurations with P^2 (resp. P^3) polynomials. This quantity varies from 0.84 to 1, i.e. 19% (resp. from 0.89 to 1, i.e. 12%). This definition is already satisfactory but it could be improved by computing the expression of the lower branch obtained for isoscele triangles and then by taking into account a third parameter, the maximum angle of the reference triangle.

5.2 Lower bound of $\gamma_{\min}\rho_{\mathbf{ins}}$

As for the upper bound of $\gamma_{\min}\rho_{\mathrm{ins}}$, we first tried to approximate the lower branch of isoscele triangle of Fig. 15 by polynomial functions of $\theta_{\min}$, but we

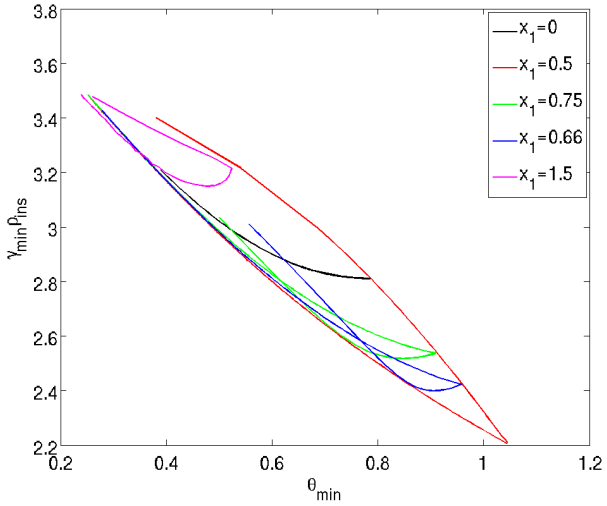

Figure 17: $\xi_F = \rho_{ins}$ for five configurations in P^3

realized that trigonometric functions were more appropriate. We found out that good approximations of this lower branch were given by

$$f_{2,1} \ : \ (\theta_{\min}) \longmapsto f_{2,1}\left(\theta_{\min}\right) = 1 - \sin\left(\frac{\theta_{\min}}{2}\right).$$

In Fig. 27, we plot $f_{2,1}$ (red line) and the lower branch (black line with +). The curves are superimposed. In Fig. 28, we plot the relative error between the two functions. This error is smaller than 1%, so that $f_{2,1}$ is a good approximation of the lower branch. For P^2 and P^3 polynomials, we found out that a good approximation of the lower branch was respectively

$$f_{2,2} \ : \ \theta_{\min} \longmapsto f_{2,2}\left(\theta_{\min}\right) = 2.68 - 0.49\cos\left(\theta_{\min}\right) - 1.41\sin\left(\theta_{\min}\right),$$

and

$$f_{2,3} =: \ \theta_{\min} \longmapsto f_{2,3}\left(\theta_{\min}\right) = 4.03 - 0.05\cos\left(\theta_{\min}\right) - 2.08\sin\left(\theta_{\min}\right),$$

In Fig, 29 (resp. Fig. 31), we represent $f_{2,2}$ (resp. $f_{2,3}$) and the lower branch for P^2 (resp. P^3) polynomials. Once again, the curves are superimposed. In Fig. 30 (resp. Fig. 32) we plot the relative error between the two functions for P^2 (resp. P^3) polynomials.

We do not plot $\dfrac{\gamma_{\min}\rho_{\text{ins}}}{f_{2,i}}$ since $\dfrac{f_{2,i}}{\rho_{\text{ins}}}$ just give a lower bound of the optimal parameter and then cannot guarantee the stability. However, we will see in the next section that coupling this quantity to a third parameter, the maximal angle of the triangle leads to a very accurate approximation of $\gamma_{\min}$.

5.3 The influence of the maximum angle

In this section, we study the influence of the maximal angle of K_0, $\theta_{\max}$ on $\gamma_{\min}$. Indeed we only considered until now two parameters, ρ_{ins} and $\theta_{\min}$, to describe

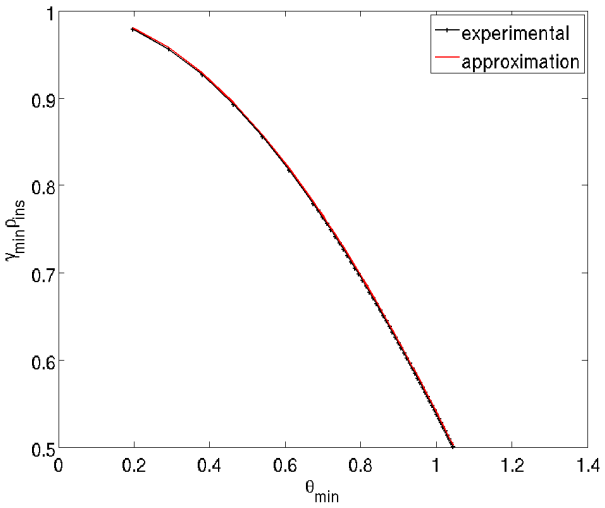

Figure 18: Comparison between the upper branch and its approximation in P^1

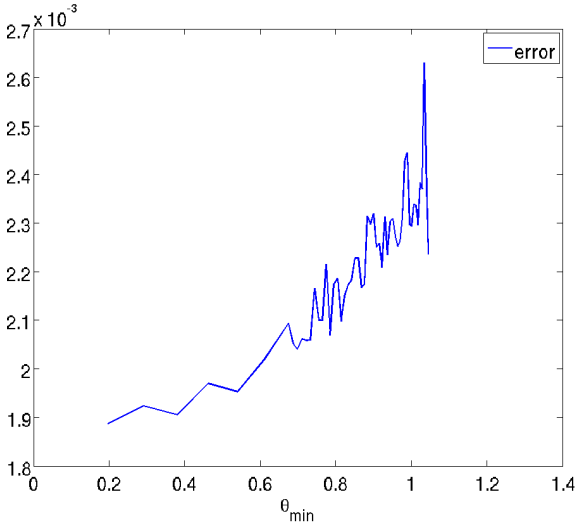

Figure 19: Relative error between the upper branch and its approximation in P^1

$\gamma_{\min}$, while a triangle is completely characterized by three parameters.
Let $\theta_{\min} \in \left[0; \frac{\pi}{3}\right]$ and we denote by θ the third angle of K_0. Obviously

$$\theta_{\min} \leq \theta \leq \theta_{\max} \text{ and } \theta_{\max} + \theta + \theta_{\min} = \pi.$$

Then, for a given $\theta_{\min}$, we have

$$\frac{\pi - \theta_{\min}}{2} \leq \theta_{\max} \leq \pi - 2\theta_{\min}.$$

The lower bound is reached when $\theta = \theta_{max}$, i.e. when K_0 is an isoscele triangle such that the base angle is greater than $\frac{\pi}{3}$ (cf figure 33). In this configuration,

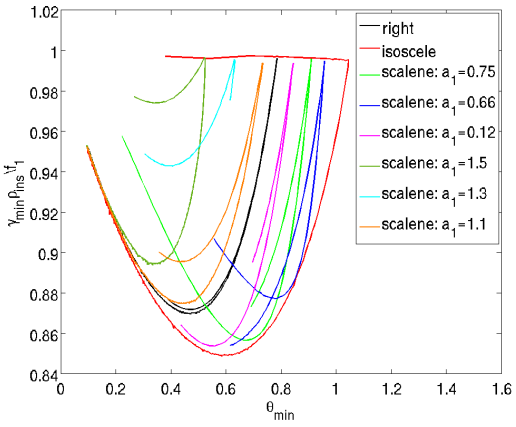

Figure 20: $\xi_F = {}^{\rho_{ins}}/_{f_1}$ for the eight configurations in P^1

we know from section 5.2 that $\gamma_{\min}\rho_{\text{ins}} \simeq f_{2,i}$. The upper bound is reached when $\theta = \theta_{\min}$, i.e. when K_0 is an isoscele triangle with a base angle smaller than $\dfrac{\pi}{3}$ (cf. figure 34). In this configuration, we know from section 5.1 that $\gamma_{\min}\rho_{\text{ins}} \simeq f_{1,i}$. Since we also know that, whatever $\theta_{\max}$,

$$f_{2,i}\left(\theta_{\min}\right) \leq \gamma_{\min}\rho_{\text{ins}} \leq f_{1,i}\left(\theta_{\min}\right)$$

we search for an approximation of $\gamma_{\min}\rho_{\text{ins}}$ under the form

$$F\left(\theta_{\max}, \theta_{\min}\right) = f_{1,i}\left(\theta_{\min}\right) + G\left(\theta_{\max}\right)\left(f_{2,i}\left(\theta_{\min}\right) - f_{1,i}\left(\theta_{\min}\right)\right).$$

where G is such that

$$\begin{cases} G\left(\dfrac{\pi - \theta_{\min}}{2}\right) = 1, \\ G\left(\pi - 2\theta_{\min}\right) = 0, \\ \\ 0 \leq G\left(\theta_{\max}\right) \leq 1, \text{ for } \dfrac{\pi - \theta_{\min}}{2} \leq \theta_{\max} \leq \pi - 2\theta_{\min}. \end{cases}$$

Once again, we first tried to express G as a polynomial function of $\theta_{\max}$ but it appeared that the most appropriate expression was

$$G = \cos\left(\Theta\right) \text{ with } \Theta = \frac{\pi}{2}\left(\frac{2\theta_{\max} - \pi + \theta_{\min}}{\pi - 3\theta_{\min}}\right).$$

In Fig. 35 we plot $\gamma_{\min}\rho_{\text{ins}}$ and its approximation by $F\left(\theta_{\min}, \theta_{\max}\right)$ for the eight configurations previously described.

For all the configurations, the curves are perfectly superimposed. In Fig. 36, we plot the relative error between $\gamma_{\min}\rho_{\text{ins}}$ and its approximation by F. For the sake of clarity we restricted ourselves to the configurations $x_1 = 0.5$; $x_1 = 0.12$; $x_1 = 1.5$ and $x_1 = 0$. But the results are similar for the three other configurations. The relative error is always smaller than 1% and we conclude that a good definition of ξ_F is

$$\xi_F = \frac{\rho_{\text{ins}}}{F\left(\theta_{\max}, \theta_{\min}\right)}.$$

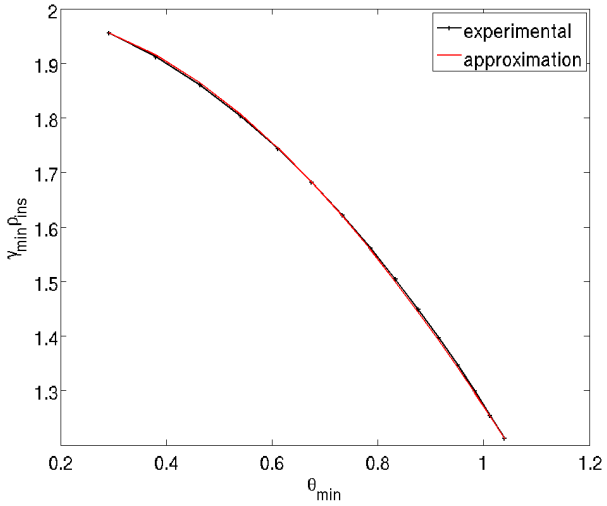

Figure 21: Comparison between the upper branch and its approximation in P^2

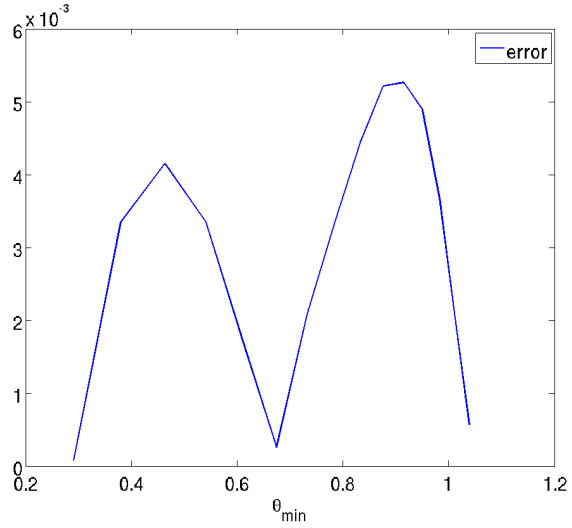

Figure 22: Relative error between the upper branch and its approximation in P^2

In Fig. 37, we plot $\frac{\gamma_{\min}\rho_{\text{ins}}}{F}$ for the eight configurations we considered. This quantity varies from 0.99 to 1 (1%) and $\frac{\rho_{\text{ins}}}{F}$ is then a better definition of ξ_F than ρ_{ins} or $\frac{\rho_{\text{ins}}}{f_1}$.

In Fig. 38 (resp. in Fig. 39), we plot $\frac{\gamma_{\min}\rho_{\text{ins}}}{F}$ for the five configurations we have considered in P^2 (resp. in P^3). This quantity varies from 0.995 to 1.04 (3%) (resp. from 0.995 to 1.008 (1%)) and here again, for P^2 and P^3 polynomials,

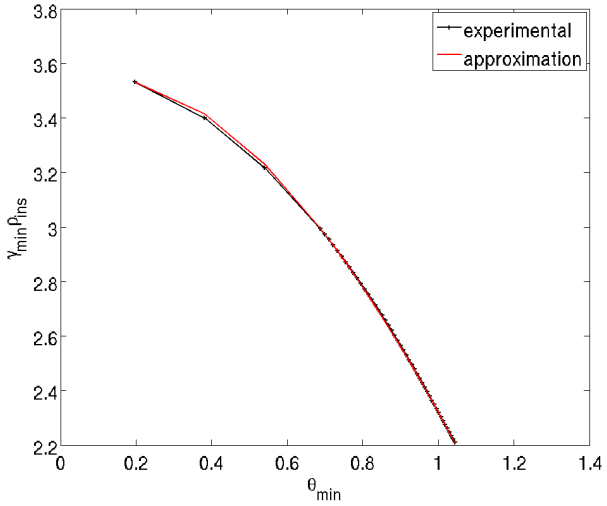

Figure 23: Comparison between the upper branch and its approximation in P^3

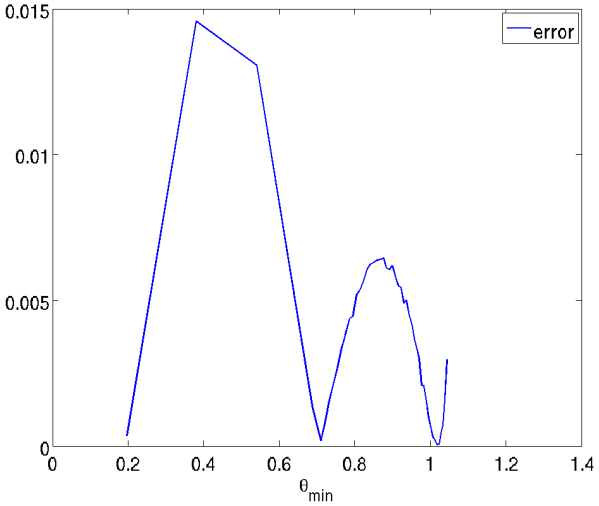

Figure 24: Relative error between the upper branch and its approximation in P^3

$\frac{\rho_{\text{ins}}}{F}$ is a better choice of ξ_F than ρ_{ins} or $\frac{\rho_{\text{ins}}}{f_1}$.
This last definition allows us to compute a penalization parameter independent of the mesh and to overcome the biggest difficulty of the IPDG method. Indeed, the classical definitions implie to modify the value of α for each mesh or to choose α large enough that is to say to over-penalize the bilinear form. Now, we have to study the influence of theses different definitions over the CFL condition for non-uniform meshes.

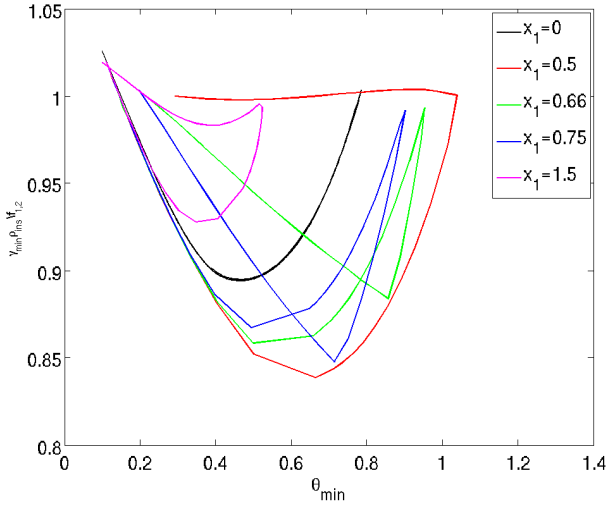

Figure 25: $\xi_F = \rho_{ins}/f_{1,2}$ for the eight configurations in P^2

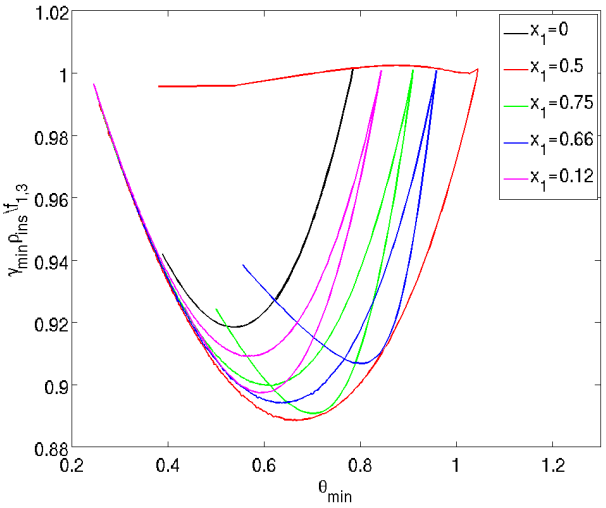

Figure 26: $\xi_F = \rho_{ins}/f_{1,3}$ for the eight configurations in P^3

6 Study of the CFL condition

In this study, we have considered four definitions for ξ_F: ρ_{circ}, ρ_{ins}, ρ_{ins}/f_1 and ρ_{ins}/F and we have concluded that the last one was the most adapted. We have also seen in [1] that the choice of the coefficient of penalization can strongly influence the stability condition of the Leap-frog scheme. So we may wonder how the four definitions modify the CFL condition. In this section, we are interested in the discretization of the square $[-1,1]^2$ by a non-uniform triangular mesh. We consider a point source in space located in $(0.5, 0.5)$. The expression of the source in time is the same as in the section 4.

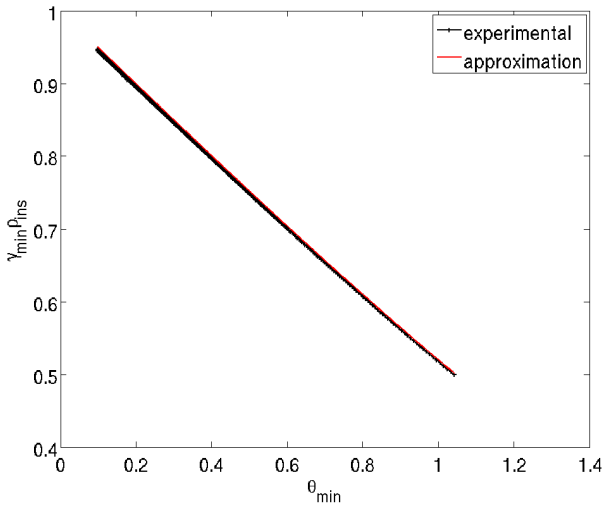

Figure 27: Comparison between the lower branch and its approximation in P^1

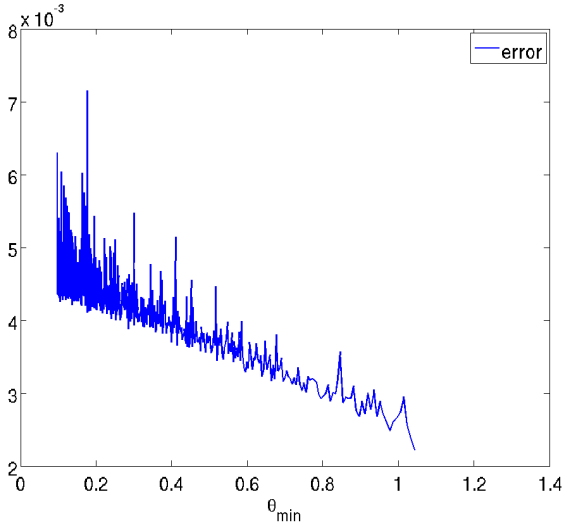

Figure 28: Relative error between the lower branch and its approximation in P^1

For each of the four definitions of ξ_F, we have numerically studied the dependence between the CFL condition and the penalization parameter γ_1. To compute the CFL condition for a fixed γ_1, we use a dichotomy method using the algorithm 2. The principle of this algorithm is similar to this of the algorithm 1: we solve the wave equation for a given time step; then we decrease the time step if the scheme explodes and we increase it else.

We represent in Fig. 40 the results obtained for P^1 polynomial and for:

- $\xi_F = \rho_{circ}$: black line,
- $\xi_F = \rho_{ins}$: red dashed and dotted line

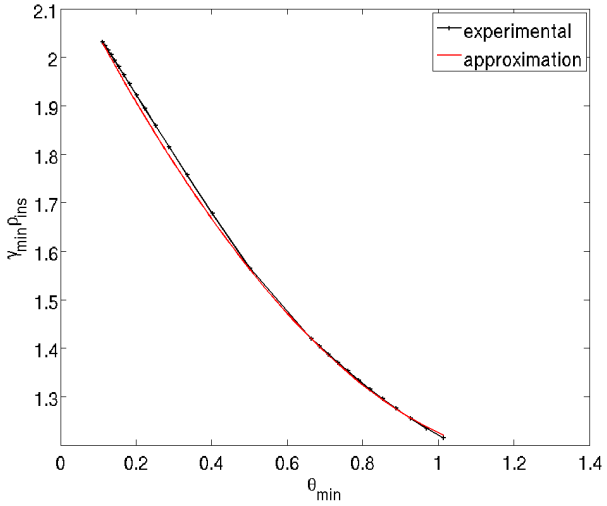

Figure 29: Comparison between the lower branch and its approximation in P^2

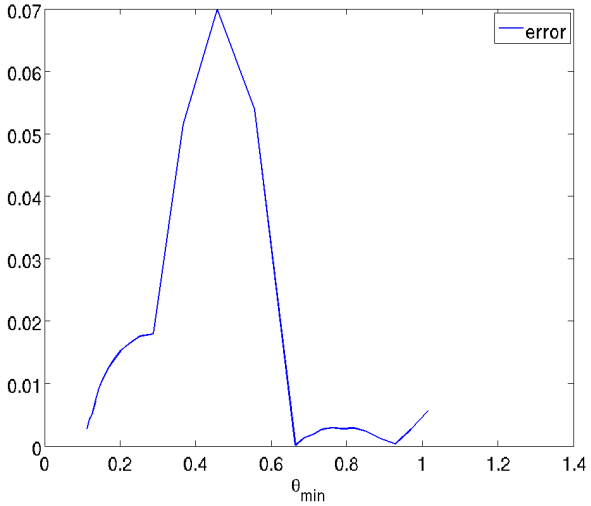

Figure 30: Relative error between the lower branch and its approximation in P^2

- $\xi_F = \dfrac{\rho_{ins}}{f_1}$: blue dashed line,
- $\xi_F = \dfrac{\rho_{ins}}{F}$: magenta dotted line.

First of all, let us remark that the optimal parameter $\alpha_{\min}$ depends on the definition of ξ_F. It is also clear in figure 40 that the three definitions ρ_{ins}, ρ_{ins}/f_1 and ρ_{ins}/F allow to reach a CFL condition greater $(5e-3)$ than with the definition ρ_{circ} $(4.1e-3)$ that is to say a time step 22% higher. However, there is no real difference between the three definitions that is why we recommend to use the definition ρ_{ins} which is the easiest to implement. In Fig. 41 (resp. Fig.

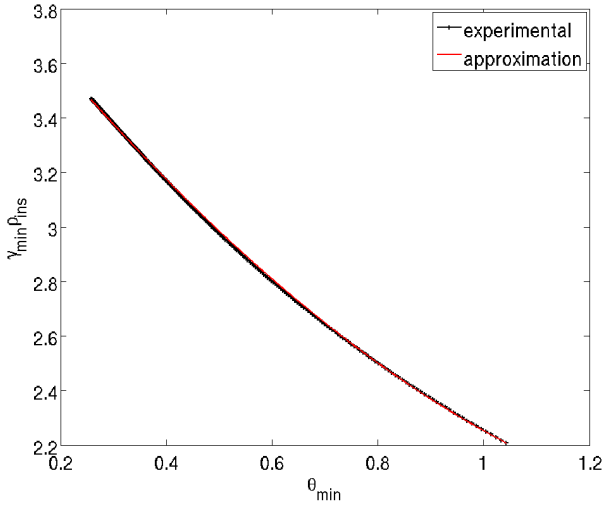

Figure 31: Comparison between the lower branch and its approximation in P^3

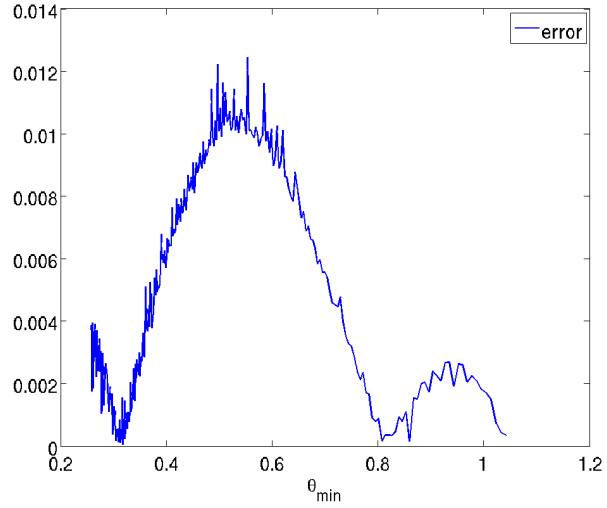

Figure 32: Relative error between the lower branch and its approximation in P^3

42), we represent the evolution of the CFL condition with respect to γ_1 for P^2 elements (resp. P^3 elements) and for:

- $\xi_F = \rho_{circ}$: black line,
- $\xi_F = \rho_{ins}$: red dashed and dotted line.

We remark that we can use a time step of $2.56e-3$ ($1.53e-3$) considering the diameter of the inscribed circle and of $1.55e-3$ ($1.05e-3$) considering the diameter of the circumcircle, which is equivalent to use a time step 65% (resp. 46%) higher.

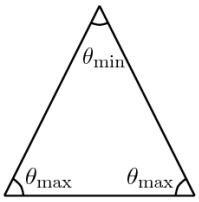

Figure 33: Isoscele triangle with $\theta = \theta_{\max}$

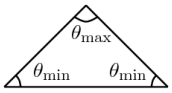

Figure 34: Isoscele triangle with $\theta = \theta_{\min}$

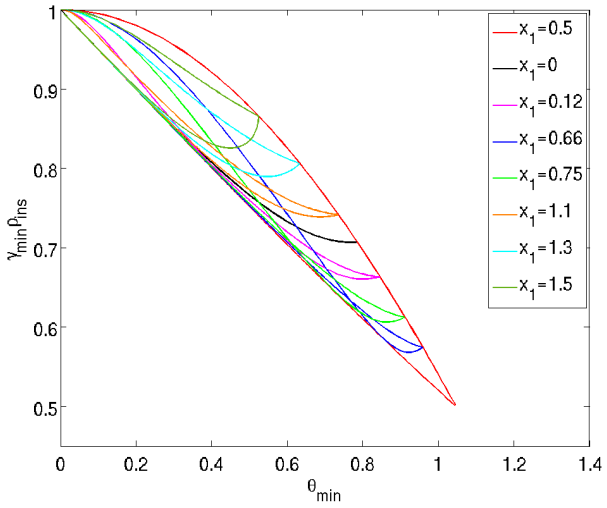

Figure 35: Comparison between $\gamma_{\min}\rho_{\text{ins}}$ and $F(\theta_{\min}, \theta_{\max})$ in P^1

Algorithm 2

$\Delta t_1 = 6.9E-3$ and $\Delta t_2 = 0.17$
$\Delta t = \dfrac{\Delta t_1 + \Delta t_2}{2}$
We compute the solution with Δt
if explosion **then**
  $\Delta t_2 = \Delta t$
else
  $\Delta t_1 = \Delta t$
end if
if $|\Delta t - \dfrac{\Delta t_1 + \Delta t_2}{2}| < 10^{-5}\Delta t$ **then**
  $\Delta_{\text{opt}} = \Delta t_1$
else
  Return in 2.
end if

We have also performed some experiments in dimension 3 considering the cube $[0,1]^3$ discretized by a non-uniform mesh composed by tetrahedrons. Due

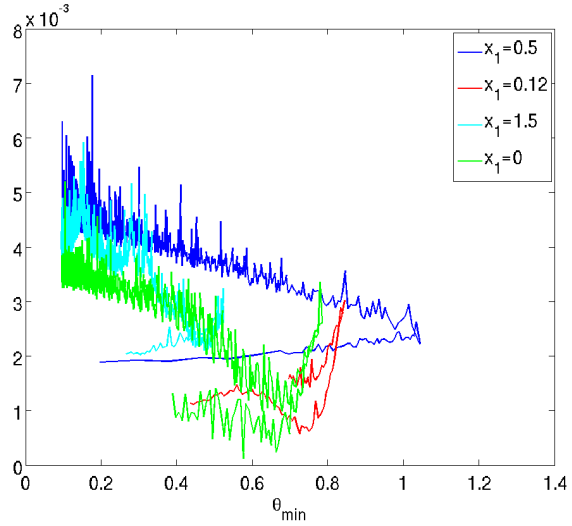

Figure 36: Error between $\gamma_{\min}\rho_{\text{ins}}$ and $F(\theta_{\min}, \theta_{\max})$

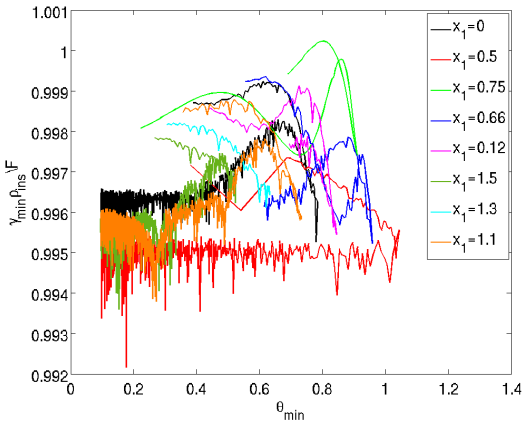

Figure 37: $\xi_F = \rho_{ins}/F$ for the eight configurations in P^1

to obvious computational cost problems, we are not able to perform a study as accurate as in the 2D case but we have obtained time steps 20% higher with P^1 elements, 25% higher with P^2 elements and 33% higher with P^3 elements using the diameter of the inscribed sphere.

7 Conclusion

In this paper, we have numerically compared the different definitions of the parameter ξ_F proposed in the litterature. As wa already observed in [1], the most appropriate choice is to consider the diameter of the inscribed circle. Indeed this choice leads to a penalization parameter much more independent of the mesh than the circumscribed circle. Nevertheless, this result is clearly not

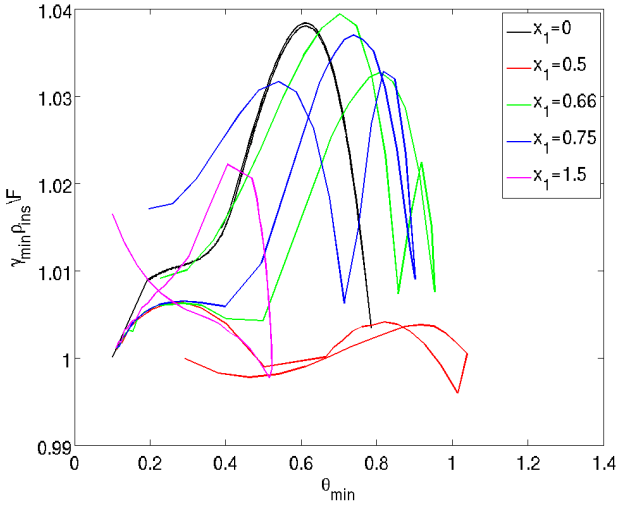

Figure 38: $\xi_F = \rho_{ins}/_F$ for the eight configurations in P^2

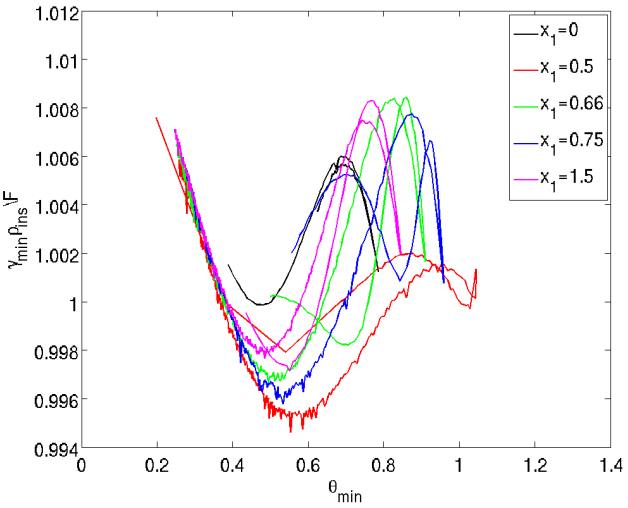

Figure 39: $\xi_F = \rho_{ins}/_F$ for the eight configurations in P^3

optimal since the parameter of penalization still strongly varies from one mesh to another (about 100%). That is why we have proposed more sophisticated expressions of ξ_F, involving the minimal and maximal angles of the cells and leading to very small variations of the penalization parameter from one mesh to another (about 1%). Using this expression, it is no longer necessary to adjust the value of the penalization parameter before each experiment to ensure the stability of the scheme. Moreover, we have also remarked that this choice strongly modifies the CFL condition. Indeed, the results of the section 6 show that the time step can be increased by 22% to 65% in 2D and by 20% to 33% in 3D, using the inscribed circle (or sphere) rather than the circumscribed one.

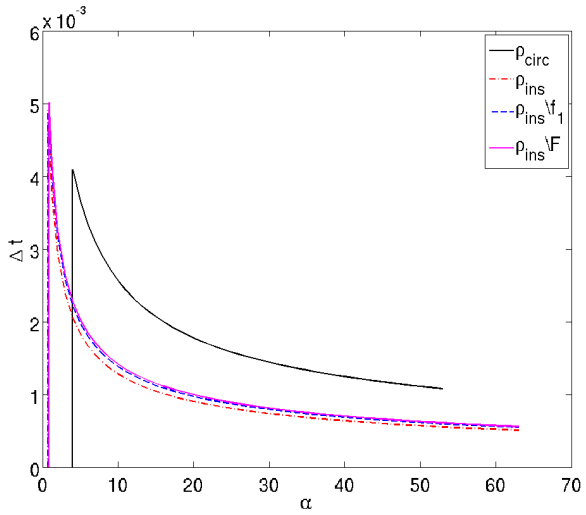

Figure 40: CFL condition for four definitions of ξ_F in P^1

This means that the number of iterations can be divided by a factor between 1.22 and 1.65.

A Stability analysis

In this section, we present the analytical results we have obtained for various triangular meshes. In order to apply a stability analysis similar to [1], we consider infinite meshes constructed from a reference element K_0 as explained in section 4. We denote by $K_{I,J}$ (resp. $K^*_{I,J}$) the translation of K_0 (resp. K^*_0) along the vector $(I + Jx_1, Jy_1)$ and by $E_{I,J}$ the macroelement $K_{I,J} \cup K^*_{I,J}$.

If we consider the wave equation totally discretized over one element $E_{I,J}$ of the mesh, we have for all $E_{I,J} \in \mathcal{T}_h$

$$M_{2,p}\frac{U^{n+1}_{I,J} - 2U^n_{I,J} + U^{n-1}_{I,J}}{\Delta t^2} + K_{2,p}U^n_{I,J} + \left(K^W_{2,p}\right)^T U^n_{I-1,J} + K^W_{2,p}U^n_{I+1,J} + \left(K^N_{2,p}\right)^T U^n_{I,J-1} + K^N_{2,p}U^n_{I,J+1} = 0 \tag{10}$$

where $U_{I,J}$ corresponds to the vector of unknown U restricted to the element $E_{I,J}$, $M_{2,p}$ (resp. $K_{2,p}$) is the mass matrix (resp. stiffness matrix) corresponding to the element $E_{I,J}$, $K^W_{2,p}$ (resp. $K^N_{2,p}$) is the stiffness matrix corresponding to the interface between the elements $E_{I,J}$ and $E_{I+1,J}$ (resp. $E_{I,J}$ and $E_{I,J+1}$) considering polynomials of degree p. All these matrices have the same size: $(2N, 2N)$ where N is the number of basis functions considered since one cell $E_{I,J}$ is composed by deux triangular elements.
Then, applying the discrete Fourier transform on (10) along the directions $(1, 0)$ and (x_1, y_1), we obtain, $\forall \beta_1, \beta_2 \in [-\pi, \pi]$

$$M_{2,p}\frac{\hat{U}^{n+1} - 2\hat{U}^n + \hat{U}^{n-1}}{\Delta t^2} + K_{\beta_1,\beta_2}\hat{U}^n = 0 \tag{11}$$

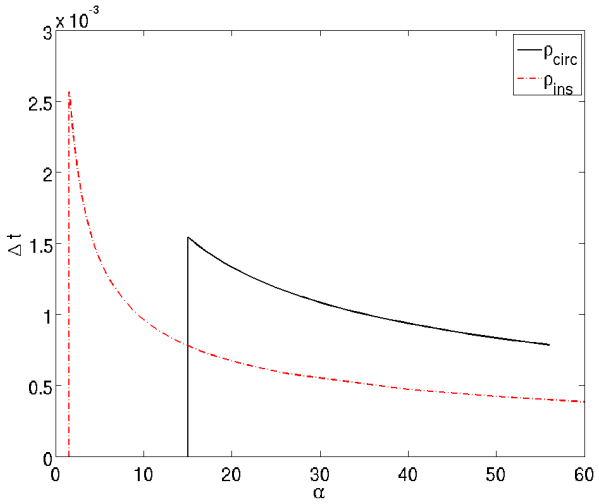

Figure 41: CFL condition for two definitions of ξ_F in P^2

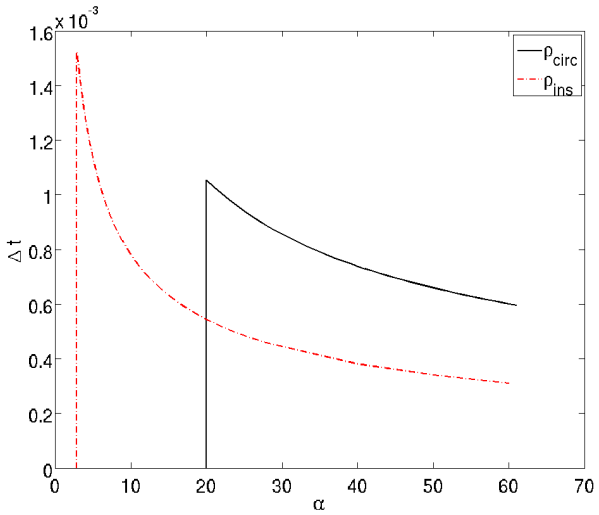

Figure 42: CFL condition for two definitions of ξ_F in P^3

where $K_{\beta_1,\beta_2} = K_{2,p} + K^W_{2,p}e^{i\beta_1} + \left(K^W_{2,p}\right)^T e^{-i\beta_1} + K^N_{2,p}e^{i\beta_2} + \left(K^N_{2,p}\right)^T e^{-i\beta_2}$.
In the same way as in [1], the stability of the scheme is ensured if and only if

$$0 \leq \lambda \leq \frac{4}{\Delta t^2}$$

with $\lambda \in \Lambda(\beta_1, \beta_2)$ where $\Lambda(\beta_1, \beta_2)$ represent the set of eigenvalues of $N_{\beta_1,\beta_2} := M^{-1}_{2,p}K_{\beta_1,\beta_2}$. A necessary and sufficient stability condition is then

$$\lambda_{\min} \geq 0 \qquad \text{et} \qquad \Delta t \leq \frac{2}{\sqrt{\lambda_{\max}}}$$

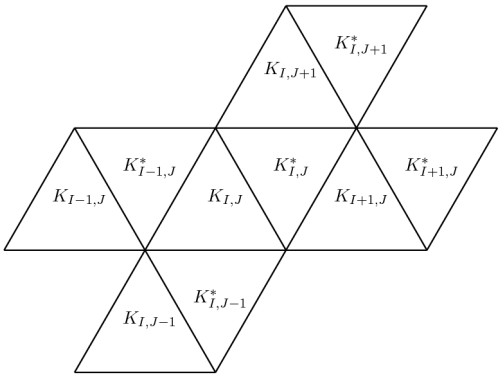

Figure 43: Neighbors of a cell $E_{I,J} = K_{I,J} \cup K^*_{I,J}$

with $\lambda_{\min} = \min_{\beta_1,\beta_2\in[-\pi,\pi]} [\min(\Lambda(\beta_1,\beta_2))]$ and $\lambda_{\max} = \max_{\beta_1,\beta_2\in[-\pi,\pi]} [\max(\Lambda(\beta_1,\beta_2))]$.

A.1 Mesh composed of equilateral triangles

In this subsection, we focus on mesh generated by equilateral triangles i.e. that we have constructed thanks to the reference triangle K_0 defined by $x_1 = 1/2$ and $y_1 = \sqrt{3}/2$.
We first give the expressions of the different matrices of (11). The mass matrix is given by

$$M_{2,p} = \begin{pmatrix} M^1_{2,p} & 0 \\ 0 & M^1_{2,p} \end{pmatrix} \qquad \text{where} \qquad M^1_{2,p} = \frac{1}{24}\begin{pmatrix} 2 & 1 & 1 \\ 1 & 2 & 1 \\ 1 & 1 & 2 \end{pmatrix}.$$

The stiffness matrices $K^W_{2,p}$ and $K^N_{2,p}$ are

$$K^W_{2,p} = \begin{pmatrix} 0 & 0 \\ K^{W,1}_{2,p} & 0 \end{pmatrix} \qquad \text{where} \qquad K^{W,1}_{2,p} = \frac{1}{6}\begin{pmatrix} \sqrt{3}-\alpha & -\sqrt{3} & \sqrt{3}-2\alpha \\ -\sqrt{3} & 0 & -\sqrt{3} \\ \sqrt{3}-2\alpha & -\sqrt{3} & \sqrt{3}-\alpha \end{pmatrix}$$

and

$$K^N_{2,p} = \begin{pmatrix} 0 & 0 \\ K^{N,1}_{2,p} & 0 \end{pmatrix} \qquad \text{where} \qquad K^{N,1}_{2,p} = \frac{1}{6}\begin{pmatrix} \sqrt{3}-\alpha & \sqrt{3}-2\alpha & -\sqrt{3} \\ \sqrt{3}-2\alpha & \sqrt{3}-\alpha & -\sqrt{3} \\ -\sqrt{3} & -\sqrt{3} & 0 \end{pmatrix}.$$

Finally, the matrix $K_{2,p}$, which is full, can be written as

$$K_{2,p} = \begin{pmatrix} K^1_{2,p} & K^2_{2,p} \\ K^2_{2,p} & K^1_{2,p} \end{pmatrix}$$

with

$$K^1_{2,p} = \frac{\alpha}{6}\begin{pmatrix} 4 & 1 & 1 \\ 1 & 4 & 1 \\ 1 & 1 & 4 \end{pmatrix}, \qquad K^2_{2,p} = \frac{1}{6}\begin{pmatrix} 0 & -\sqrt{3} & -\sqrt{3} \\ -\sqrt{3} & \sqrt{3}-\alpha & \sqrt{3}-2\alpha \\ -\sqrt{3} & \sqrt{3}-2\alpha & \sqrt{3}-\alpha \end{pmatrix}.$$

The study of the eigenvalues of the matrix N_{β_1,β_2} is very complicated for all β_1 and β_2 so we restrict ourselves to the cases $\beta_1 = \beta_2 = 0$ and $\beta_1 = \beta_2 = \pi$ in order to obtain a necessary condition of stability.

- In the case where $\beta_1 = \beta_2 = 0$, the characteristic polynomial $p_\alpha(\lambda, \beta_1, \beta_2)$ of the matrix N_{β_1,β_2} is given by

$$p_\alpha(\lambda, 0, 0) = \lambda^6 + \sum_{i=0}^{5} c_i(\alpha, 0, 0)\,\lambda^i$$

where the coefficients $c_i(\alpha, 0, 0)$ are defined by

$$\begin{cases} c_5(\alpha,0,0) = & -60\alpha, \\ c_4(\alpha,0,0) = & 288\left(5\alpha^2 - 3\right), \\ c_3(\alpha,0,0) = & 3456\alpha\left(9 - 5\alpha^2\right), \\ c_2(\alpha,0,0) = & 20736\left(9 - 18\alpha^2 + 5\alpha^4\right), \\ c_1(\alpha,0,0) = & 248832\alpha\left(-9 + 6\alpha^2 - \alpha^5\right), \\ c_0(\alpha,0,0) = & 0. \end{cases}$$

We are going to use the Descarte's rule of signs to study the positivity of the eigenvalues of the matrix $N_{0,0}$. We briefly present the results obtained for each coefficient $c_i(\alpha, 0, 0)$, the method employed is the same as the one used in [1]. We recall that we are seeking conditions for $\alpha \in \mathbb{R}^+$.

  - $-c_5(\alpha, 0, 0) \geq 0$ is always true,
  - $c_4(\alpha, 0, 0) \geq 0 \Leftrightarrow \alpha \geq \dfrac{\sqrt{15}}{5}$,
  - $-c_3(\alpha, 0, 0) \geq 0 \Leftrightarrow \alpha \geq \dfrac{3\sqrt{5}}{5}$,
  - $c_2(\alpha, 0, 0) \geq 0 \Leftrightarrow \alpha \geq \sqrt{3}$,
  - $-c_1(\alpha, 0, 0) \geq 0 \Leftrightarrow \alpha \geq \sqrt{3}$.

Consequently, the eigenvalues of the matrix $N_{0,0}$ are positive if and only if

$$\alpha \geq \sqrt{3} \simeq 1.73. \tag{12}$$

- Let us focus on the case where $\beta_1 = \beta_2 = \pi$, then the characteristic polynomial of the matrix N_{β_1,β_2} is given by

$$p_\alpha(\lambda, \pi, \pi) = \lambda^6 + \sum_{i=0}^{5} c_i(\alpha, \pi, \pi)\,\lambda^i$$

where the coefficients $c_i(\alpha,\pi,\pi)$ are defined by

$$\begin{cases} c_5(\alpha,\pi,\pi) = & -60\alpha, \\ c_4(\alpha,\pi,\pi) = & 8\left(160\alpha^2+72\sqrt{3}\alpha-183\right), \\ c_3(\alpha,\pi,\pi) = & -288\alpha\left(40\alpha^2+76\sqrt{3}\alpha-191\right), \\ c_2(\alpha,\pi,\pi) = & 48\left(848\alpha^4+4944\sqrt{3}\alpha^3-6088\alpha^2-9648\sqrt{3}\alpha+10731\right), \\ c_1(\alpha,\pi,\pi) = & -576\alpha\left(80\alpha^4+1216\sqrt{3}\alpha^3+5712\alpha^2-13608\sqrt{3}\alpha+15387\right), \\ c_0(\alpha,\pi,\pi) = & 4608\left(120\sqrt{3}\alpha^5+1676\alpha^4-810\sqrt{3}\alpha^3-11753\alpha^2\right. \\ & \left.+11052\sqrt{3}\alpha-7776\right). \end{cases}$$

From this case, we just present the result obtained from the most restrictive condition in order to simplify the presentation of the results. The study of the sign of each coefficient $c_i(\alpha,\pi,\pi)$ show that the eigenvalues of the matrix $N_{\pi,\pi}$ are positive if and only if

$$\alpha \geq \frac{9\sqrt{3}}{10} \simeq 1.56. \tag{13}$$

- Finally, we consider the case $\beta_1 = 0$, $\beta_2 = \pi$, which is equivalent to the case $\beta_1 = \pi$, $\beta_2 = 0$. With such a choice of β_1 and β_2, the matrix $N_{0,\pi}$ admits as characteristic polynomial

$$p_\alpha(\lambda,0,\pi) = \lambda^6 + \sum_{i=0}^{5} c_i(\alpha,0,\pi)\,\lambda^i$$

with the coefficients $c_i(\alpha,0,\pi)$:

$$\begin{cases} c_5(\alpha,\pi,\pi) = & -60\alpha, \\ c_4(\alpha,\pi,\pi) = & 1280\alpha^2+384\sqrt{3}\alpha-672, \\ c_3(\alpha,\pi,\pi) = & -11520\alpha^3-14592\sqrt{3}\alpha^2+25344\alpha, \\ c_2(\alpha,\pi,\pi) = & 40704\alpha^4+158208\sqrt{3}\alpha^3-141312\alpha^2-142848\sqrt{3}\alpha+112896, \\ c_1(\alpha,\pi,\pi) = & -46080\alpha^5-466944\sqrt{3}\alpha^4-1419264\alpha^3+2433024\sqrt{3}\alpha^2-1963008\alpha, \\ c_0(\alpha,\pi,\pi) = & 368640\sqrt{3}\alpha^5+3391488\alpha^4-1327104\sqrt{3}\alpha^3-11206656\alpha^2 \\ & +7741440\sqrt{3}\alpha-3981312. \end{cases}$$

The study of these coefficients leads to the same conclusion as for the previous case i.e. the eigenvalues of $N_{0,\pi}$ are positive if and only if

$$\alpha \geq \frac{3\sqrt{3}}{5} \simeq 1.04. \tag{14}$$

Then, combining the conditions (12) and (13), we obtain as necessary condition that the L^2 stability of the scheme is ensured if $\alpha \geq \sqrt{3}$.

Remark A.1. *The numerical experiments we have performed over such meshes confirm this results since, numerically, we have stability for* $\alpha \geq 1.74$. *It seems that the case* $\beta_1 = \beta_2 = 0$ *is the critical case which allows to conclude to the stability of the scheme.*

A.2 Mesh composed of right triangles

In this subsection, we consider for reference triangle the triangle K_0 with $x_1 = 0$ and $y_1 = 1$ which leads to a mesh composed of right isoscele triangles.
In such a configuration, the mass matrix is the same as the one of the subsection A.1 and the stiffness matrices $K_{2,p}^W$ and $K_{2,p}^N$ are given by

$$K_{2,p}^W = \begin{pmatrix} 0 & 0 \\ K_{2,p}^{W,1} & 0 \end{pmatrix} \qquad \text{where} \qquad K_{2,p}^{W,1} = \frac{1}{12}\begin{pmatrix} -2\alpha+6 & -3 & -4\alpha+3 \\ -3 & 0 & -3 \\ -4\alpha+3 & -3 & -2\alpha \end{pmatrix}$$

and

$$K_{2,p}^N = \begin{pmatrix} 0 & 0 \\ K_{2,p}^{N,1} & 0 \end{pmatrix} \qquad \text{where} \qquad K_{2,p}^{N,1} = \frac{1}{12}\begin{pmatrix} -2\alpha+6 & -4\alpha+3 & -3 \\ -4\alpha+3 & -2\alpha & -3 \\ -3 & -3 & 0 \end{pmatrix}.$$

The matrix $K_{2,p}$ is under the form

$$K_{2,p} = \begin{pmatrix} K_{2,p}^1 & K_{2,p}^2 \\ K_{2,p}^2 & K_{2,p}^1 \end{pmatrix}$$

with

$$K_{2,p}^1 = \frac{\alpha}{6}\begin{pmatrix} 4 & 1 & 1 \\ 1 & 2\left(1+\sqrt{2}\right) & \sqrt{2} \\ 1 & \sqrt{2} & 2\left(1+\sqrt{2}\right) \end{pmatrix}, \qquad K_{2,p}^2 = \frac{1}{12}\begin{pmatrix} 0 & -6 & -6 \\ -12 & -2\alpha\sqrt{2}+6 & -4\alpha\sqrt{2}+6 \\ -12 & -4\alpha\sqrt{2}+6 & -2\alpha\sqrt{2}+6 \end{pmatrix}.$$

Let us now study the positivity of the eigenvalues of the matrix N_{β_1,β_2} in the same cases as in subsection A.1.

- We assume that $\beta_1 = \beta_2 = 0$. In this case, the characteristic polynomial of the matrix $N_{0,0}$ is given by

$$p_\alpha(\lambda, 0, 0) = \lambda^6 + \sum_{i=0}^{5} c_i(\alpha, 0, 0)\,\lambda^i$$

where the coefficients $c_i(\alpha,0,0)$ are given by

$$\begin{cases} c_5(\alpha,0,0) = & -20\left(2+\sqrt{2}\right)\alpha, \\ c_4(\alpha,0,0) = & 768\left(1+\sqrt{2}\right)\alpha^2 + 192\left(\sqrt{2}-1\right)\alpha - 1440, \\ c_3(\alpha,0,0) = & -10368\left(1+\sqrt{2}\right)\alpha^3 + 1152\left(3-4\sqrt{2}\right)\alpha^2 + 17280\left(\sqrt{2}+2\right)\alpha, \\ c_2(\alpha,0,0) = & 6912\left(13+8\sqrt{2}\right)\alpha^4 + 27648\sqrt{2}\alpha^3 - 138240\left(2\sqrt{2}+3\right)\alpha^2 \\ & +82944\left(\sqrt{2}-1\right)\alpha + 186624, \\ c_1(\alpha,0,0) = & -82944\left(\sqrt{2}+4\right)\alpha^5 - 165888\alpha^4 + 829440\left(3+\sqrt{2}\right)\alpha^3 \\ & -497664\alpha^2 - 746496\left(\sqrt{2}+2\right)\alpha, \\ c_0(\alpha,0,0) = & 0. \end{cases}$$

Studying the sign of each coefficient $c_i(\alpha,0,0)$, we obtain that the eigenvalues of the matrix $N_{0,0}$ are positive if and only if

$$\alpha \geq 1+\sqrt{2} \simeq 2.41. \tag{15}$$

- If $\beta_1 = \beta_2 = \pi$, then $N_{\pi,\pi}$ admits for characteristic polynomial

$$p_\alpha(\lambda,\pi,\pi) = \lambda^6 + \sum_{i=0}^{5} c_i(\alpha,\pi,\pi)\lambda^i$$

where the coefficients $c_i(\alpha,0,0)$ are given by

$$\begin{cases} c_5(\alpha,\pi,\pi) = & -20\left(2+\sqrt{2}\right)\alpha \\ c_4(\alpha,\pi,\pi) = & 32\left(24+19\sqrt{2}\right)\alpha^2 + 384\left(\sqrt{2}+1\right)\alpha - 864 \\ c_3(\alpha,\pi,\pi) = & -384\left(19+16\sqrt{2}\right)\alpha^3 - 1152\left(15+14\sqrt{2}\right)\alpha^2 + 2304\left(4\sqrt{2}+11\right)\alpha \\ c_2(\alpha,\pi,\pi) = & 768\left(37+30\sqrt{2}\right)\alpha^4 + 4608\left(41\sqrt{2}+50\right)\alpha^3 - 4608\left(17\sqrt{2}+36\right)\alpha^2 \\ & -13824\left(11\sqrt{2}+14\right)\alpha + 186624 \\ c_1(\alpha,\pi,\pi) = & -9216\left(3\sqrt{2}+4\right)\alpha^5 - 18432\left(47+36\sqrt{2}\right)\alpha^4 - 55296\left(23+15\sqrt{2}\right)\alpha^3 \\ & +165888\left(23+20\sqrt{2}\right)\alpha^2 - 82944\left(11\sqrt{2}+34\right)\alpha \\ c_0(\alpha,\pi,\pi) = & 221184\left(3\sqrt{2}+4\right)\alpha^5 + 884736\left(5+3\sqrt{2}\right)\alpha^4 - 1327104\left(1+3\sqrt{2}\right)\alpha^3 \\ & -1327104\left(10\sqrt{2}+9\right)\alpha^2 + 1990656\left(7\sqrt{2}+10\right)\alpha - 11943936 \end{cases}$$

The study of the sign of each coefficient $c_i(\alpha,\pi,\pi)$ permits to say that the eigenvalues of the matrix $N_{0,0}$ are positive if and only if

$$\alpha \geq \frac{1}{2}\left(\sqrt{9+12\sqrt{2}}-3\right) \simeq 1.05. \tag{16}$$

- Finally, let us focus on the case $\beta_1 = 0$ and $\beta_2 = \pi$. In this case, the matrix $N_{0,\pi}$ has for characteristic polynomial

$$p_\alpha(\lambda, 0, \pi) = \lambda^6 + \sum_{i=0}^{5} c_i(\alpha, 0, \pi)\,\lambda^i$$

where the coefficients $c_i(\alpha, 0, \pi)$ are given by

$$\begin{cases} c_5(\alpha,0,\pi) = & -20\left(2+\sqrt{2}\right)\alpha \\ c_4(\alpha,0,\pi) = & 688\left(1+\sqrt{2}\right)\alpha^2 + 96\left(3\sqrt{2}+5\right)\alpha - 1152 \\ c_3(\alpha,0,\pi) = & -384\left(19+18\sqrt{2}\right)\alpha^3 - 384\left(40+41\sqrt{2}\right)\alpha^2 + 1152\left(11\sqrt{2}+26\right)\alpha \\ c_2(\alpha,0,\pi) = & 768\left(57+23\sqrt{2}\right)\alpha^4 + 2304\left(81\sqrt{2}+80\right)\alpha^3 - 2304\left(57\sqrt{2}+74\right)\alpha^2 \\ & -6912\left(13\sqrt{2}+40\right)\alpha + 165888 \\ c_1(\alpha,0,\pi) = & -9216\left(\sqrt{2}+8\right)\alpha^5 - 313344\left(3+\sqrt{2}\right)\alpha^4 - 55296\left(9+20\sqrt{2}\right)\alpha^3 \\ & +55296\left(63+52\sqrt{2}\right)\alpha^2 - 165888\left(6\sqrt{2}+11\right)\alpha \\ c_0(\alpha,0,\pi) = & 110592\left(\sqrt{2}+8\right)\alpha^5 + 110592\left(45+11\sqrt{2}\right)\alpha^4 - 331776\left(24+5\sqrt{2}\right)\alpha^3 \\ & -331776\left(8\sqrt{2}+15\right)\alpha^2 + 1990656\left(\sqrt{2}+5\right)\alpha - 2985984 \end{cases}$$

Considering all the previous conditions over the signs of the coefficients, $N_{0,\pi}$ is positive if and only if

$$\alpha \geq \frac{1}{62}\left(17 + 25\sqrt{2} + \sqrt{1911 - 638\sqrt{2}}\right) \simeq 1.36. \tag{17}$$

If we combine the conditions (15) to (17), a necessary condition to ensure that the eigenvalues of N_{β_1,β_2} are positive is that

$$\alpha \geq 1 + \sqrt{2}.$$

Remark A.2. *The numerical experiments we have performed over such meshes numerically confirm this result since we have stability for $\alpha \geq 2.42$. Once again, it seems that the case $\beta_1 = \beta_2 = 0$ is the critical case which permits to conclude the stability of the scheme.*

A.3 Mesh composed of scalene triangles

In this subsection, we consider for reference triangle the triangle K_0 with $x_1 = 3/4$ and $y_1 = 1$ which give mesh composed by isoscele right triangles.
Here again, the mass matrix is the same as the one in subsection A.1 and the

stiffnes matrices $K_{2,p}^W$ and $K_{2,p}^N$ are given by

$$K_{2,p}^W = \begin{pmatrix} 0 & 0 \\ K_{2,p}^{W,1} & 0 \end{pmatrix} \qquad \text{where} \qquad K_{2,p}^{W,1} = \begin{pmatrix} -\frac{5}{24}\alpha + \frac{13}{32} & -\frac{25}{64} & -\frac{5}{12}\alpha + \frac{25}{64} \\ -\frac{25}{64} & 0 & -\frac{25}{64} \\ -\frac{5}{12}\alpha + \frac{25}{64} & -\frac{25}{64} & -\frac{5}{23}\alpha + \frac{3}{8} \end{pmatrix}$$

and

$$K_{2,p}^N = \begin{pmatrix} 0 & 0 \\ K_{2,p}^{N,1} & 0 \end{pmatrix} \qquad \text{where} \qquad K_{2,p}^{N,1} = \frac{1}{24}\begin{pmatrix} -4\alpha + 3 & -8\alpha + 6 & -6 \\ -8\alpha + 6 & -4\alpha + 9 & -6 \\ -6 & -6 & 0 \end{pmatrix}.$$

The matrix $K_{2,p}$ is like

$$K_{2,p} = \begin{pmatrix} K_{2,p}^1 & K_{2,p}^2 \\ K_{2,p}^2 & K_{2,p}^1 \end{pmatrix}$$

with

$$K_{2,p}^1 = \frac{\alpha}{24}\begin{pmatrix} 18 & 4 & 5 \\ 4 & 2\left(4+\sqrt{17}\right) & \sqrt{17} \\ 5 & \sqrt{17} & 2\left(5+\sqrt{17}\right) \end{pmatrix}$$

and

$$K_{2,p}^2 = \begin{pmatrix} 0 & -\frac{17}{64} & -\frac{17}{64} \\ -\frac{17}{64} & -\frac{1}{24}\alpha\sqrt{17} + \frac{13}{32} & -\frac{1}{12}\alpha\sqrt{17} + \frac{17}{64} \\ -\frac{17}{64} & -\frac{1}{12}\alpha\sqrt{17} + \frac{17}{64} & -\frac{1}{24}\alpha\sqrt{17} + \frac{1}{8} \end{pmatrix}.$$

Let us study the positivity of the eigenvalues of the matrix N_{β_1,β_2} in the same cases as in the subsection A.1.

- We assume that $\beta_1 = \beta_2 = 0$. In this case, the characteristic polynomial of the matrix $N_{0,0}$ is given by

$$p_\alpha(\lambda, 0, 0) = \lambda^6 + \sum_{i=0}^{5} c_i(\alpha, 0, 0)\,\lambda^i$$

where the coefficients $c_i(\alpha,0,0)$ are given by

$$\begin{cases} c_5(\alpha,0,0) = & -5\left(9+\sqrt{17}\right)\alpha, \\ c_4(\alpha,0,0) = & 36\left(23+6\sqrt{17}\right)\alpha^2+\frac{3}{2}\left(45-\sqrt{17}\right)\alpha-\frac{4113}{4}, \\ c_3(\alpha,0,0) = & -36\left(333+121\sqrt{17}\right)\alpha^3+\frac{9}{2}\left(59-63\sqrt{17}\right)\alpha^2+\frac{12339}{4}\left(\sqrt{17}+9\right)\alpha, \\ c_2(\alpha,0,0) = & 243\left(273+80\sqrt{17}\right)\alpha^4+\frac{81}{2}\left(311\sqrt{17}-1005\right)\alpha^3 \\ & -\frac{27}{8}\left(17343\sqrt{17}+85951\right)\alpha^2+648\left(45-7\sqrt{17}\right)\alpha+186624, \\ c_1(\alpha,0,0) = & -1620\left(20\sqrt{17}+153\right)\alpha^5+810\left(425-117\sqrt{17}\right)\alpha^4 \\ & +\frac{81}{2}\left(32949+5933\sqrt{17}\right)\alpha^3+1944\left(99\sqrt{17}-485\right)\alpha^2 \\ & -186624\left(\sqrt{17}+9\right)\alpha, \\ c_0(\alpha,0,0) = & 0. \end{cases}$$

Let us study the sign of each coefficient $c_i(\alpha,0,0)$, we obtain that the eigenvalues of the matrix $N_{0,0}$ are positive if and only if

$$\alpha \geq \frac{1}{8}\left(9+\sqrt{17}+\frac{3}{85}\sqrt{37570-7310\sqrt{17}}\right) \simeq 2.02. \tag{18}$$

- If $\beta_1=\beta_2=\pi$, then $N_{\pi,\pi}$ admits for characteristic polynomial

$$p_\alpha(\lambda,\pi,\pi) = \lambda^6+\sum_{i=0}^{5} c_i(\alpha,\pi,\pi)\,\lambda^i$$

where the coefficients $c_i(\alpha,0,0)$ are given by

$$\left\{\begin{array}{rl}
c_5(\alpha,\pi,\pi) = & -5\left(9+\sqrt{17}\right)\alpha,\\
c_4(\alpha,\pi,\pi) = & 9\left(92+19\sqrt{17}\right)\alpha^2+3\left(29\sqrt{17}+135\right)\alpha-\frac{6561}{8},\\
c_3(\alpha,\pi,\pi) = & -45\left(7155+1935\sqrt{17}\right)\alpha^3-27\left(\frac{1137}{2}+145\sqrt{17}\right)\alpha^2\\
& +\frac{9}{8}\left(2135\sqrt{17}+20799\right)\alpha,\\
c_2(\alpha,\pi,\pi) = & 3\left(8411+2700\sqrt{17}\right)\alpha^4+\frac{9}{4}\left(21073\sqrt{17}+76689\right)\alpha^3\\
& -\frac{27}{4}\left(3609\sqrt{17}+17339\right)\alpha^2-\frac{27}{16}\left(20689\sqrt{17}+95139\right)\alpha+\frac{32673537}{256},\\
c_1(\alpha,\pi,\pi) = & -540\left(20\sqrt{17}+51\right)\alpha^5-9\left(\frac{111979}{2}+17280\sqrt{17}\right)\alpha^4\\
& -\frac{27}{16}\left(622791+112795\sqrt{17}\right)\alpha^3 s+\frac{81}{8}\left(\frac{983053}{4}+74013\sqrt{17}\right)\alpha^2\\
& -\frac{81}{256}\left(250073\sqrt{17}+6564321\right)\alpha,\\
c_0(\alpha,\pi,\pi) = & 6885\left(20\sqrt{17}+51\right)\alpha^5+\frac{459}{4}\left(\frac{80971}{4}+5805\sqrt{17}\right)\alpha^4\\
& +\frac{1377}{64}\left(8343-59041\sqrt{17}\right)\alpha^3-\frac{4131}{64}\left(\frac{123873}{4}\sqrt{17}+42871\right)\alpha^2\\
& +\frac{4131}{4}\left(1057\sqrt{17}+8271\right)\alpha-3370896.
\end{array}\right.$$

The study of the sign of each coefficient $c_i(\alpha,\pi,\pi)$ leads to the fact that the eigenvalues of the matrix $N_{0,0}$ are positive if and only if

$$\alpha \geq \frac{3311}{1976}-\frac{160}{741}\sqrt{17}+\frac{1}{5928}\sqrt{80990249-18599424\sqrt{17}} \simeq 1.14. \quad (19)$$

- Finally, let us look at the case $\beta_1 = 0$ and $\beta_2 = \pi$. In this case, the matrix $N_{0,\pi}$ has for characteristic polynomial

$$p_\alpha(\lambda,0,\pi) = \lambda^6 + \sum_{i=0}^{5} c_i(\alpha,0,\pi)\,\lambda^i$$

where the coefficients $c_i(\alpha, 0, \pi)$ are given by

$$\begin{cases} c_5(\alpha,\pi,\pi) = & -5\left(9+\sqrt{17}\right)\alpha, \\ c_4(\alpha,\pi,\pi) = & 28\left(26+7\sqrt{17}\right)\alpha^2 + \frac{27}{4}\left(7\sqrt{17}+139\right)\alpha - \frac{29817}{16}, \\ c_3(\alpha,\pi,\pi) = & -15\left(401+149\sqrt{17}\right)\alpha^3 - \frac{9}{4}\left(11135+2333\sqrt{17}\right)\alpha^2 \\ & +\frac{9}{16}\left(11199\sqrt{17}+87551\right)\alpha, \\ c_2(\alpha,\pi,\pi) = & 3\left(10941+2140\sqrt{17}\right)\alpha^4 + \frac{27}{4}\left(12527\sqrt{17}+29131\right)\alpha^3 \\ & -\frac{9}{32}\left(277789\sqrt{17}+618877\right)\alpha^2 - 324\left(174\sqrt{17}+2275\right)\alpha + 557280, \\ c_1(\alpha,\pi,\pi) = & -540\left(20\sqrt{17}+51\right)\alpha^5 - 9\left(\frac{111979}{2}+17280\sqrt{17}\right)\alpha^4 \\ & -\frac{27}{16}\left(622791+112795\sqrt{17}\right)\alpha^3 + \frac{81}{8}\left(\frac{983053}{4}+74013\sqrt{17}\right)\alpha^2 \\ & -\frac{81}{256}\left(250073\sqrt{17}+6564321\right)\alpha, \\ c_0(\alpha,\pi,\pi) = & 3240\left(20\sqrt{17}+323\right)\alpha^5 + 297\left(14607+5395\sqrt{17}\right)\alpha^4 \\ & -486\left(27323+931\sqrt{17}\right)\alpha^3 - 648\left(13123\sqrt{17}+24291\right)\alpha^2 \\ & +3732480\left(2\sqrt{17}+13\right)\alpha - 26873856. \end{cases}$$

Considering each coefficient, $N_{0,\pi}$ is positive if and only if

$$\alpha \geq \frac{1}{34422}\left(19183+5011\sqrt{17}+\sqrt{1191400986-184462342\sqrt{17}}\right) \simeq 1.76. \tag{20}$$

If we combine conditions (18) to (20), a necessary condition to ensure that the eigenvalues of N_{β_1,β_2} are positive is

$$\alpha \geq \frac{1}{8}\left(9+\sqrt{17}+\frac{3}{85}\sqrt{37570-7310\sqrt{17}}\right).$$

Remark A.3. *The numerical experiment that we have done considering such meshes confirm this result because we have stability when $\alpha \geq 2.02$. It seems that we can conclude that the scheme is stable in the critical case $\beta_1 = \beta_2 = 0$.*

B Definition of $Q_{p,\alpha}$ and $\tilde{Q}_{p,\alpha}$

We present here the expresions of the polynomial $Q_{p,\alpha}$ and of the rational function $\tilde{Q}_{p,\alpha}$ for $1 \leq p \leq 5$.

- For polynomials of degree 1, $\tilde{Q}_{p,\alpha}$ is defined by

$$\tilde{Q}_{p,\alpha}(\lambda) = \frac{h^2\lambda}{2}\left(\frac{\alpha}{3}-1\right)+\alpha.$$

Moreover we have

$$Q_{p,\alpha}(\lambda) = \sum_{i=0}^{2} \lambda^i h^{2i} \tilde{c}_i(\alpha)$$

with

$$\begin{cases} \tilde{c}_0(\alpha) = & 36\left(\alpha^2 - 2\alpha + 1\right), \\ \tilde{c}_1(\alpha) = & 12\left(\alpha^2 - \alpha\right), \\ \tilde{c}_2(\alpha) = & \alpha^2 - 6\alpha + 6, \end{cases}$$

- In the case $p = 2$, the definition of $\tilde{Q}_{p,\alpha}$ is

$$\tilde{Q}_{p,\alpha}(\lambda) = -\frac{(\alpha - 1) h^4\lambda^2 + 4(15 + 4\alpha) h^2\lambda + 240(\alpha - 3)}{24(h^2\lambda + 20)}.$$

The polynomial $Q_{p,\alpha}$ is

$$Q_{p,\alpha}(\lambda) = \sum_{i=0}^{4} \lambda^i h^{2i} \tilde{c}_i(\alpha)$$

with

$$\begin{cases} \tilde{c}_0(\alpha) = & 57600\left(\alpha^2 - 2\alpha + 1\right), \\ \tilde{c}_1(\alpha) = & 1920\left(4\alpha^2 - 43\alpha + 39\right), \\ \tilde{c}_2(\alpha) = & 16\left(46\alpha^2 - 342\alpha + 1521\right), \\ \tilde{c}_3(\alpha) = & 8\left(4\alpha^2 + \alpha - 140\right), \\ \tilde{c}_4(\alpha) = & \alpha^2 - 16\alpha + 56. \end{cases}$$

- For $p = 3$, we have $\tilde{Q}_{p,\alpha}$ defined by

$$\tilde{Q}_{p,\alpha}(\lambda) = \frac{(\alpha - 15) h^6\lambda^3 + 30(23 + \alpha) h^4\lambda^2 + 360(3\alpha - 65) h^2\lambda + 25200(\alpha - 3)}{60(h^4\lambda^2 + 48h^2\lambda + 1260)}$$

and

$$Q_{p,\alpha}(\lambda) = \sum_{i=0}^{6} \lambda^i h^{2i} \tilde{c}_i(\alpha)$$

with

$$\begin{cases} \tilde{c}_0(\alpha) = & 635040000\left(\alpha^2 - 12\alpha + 36\right), \\ \tilde{c}_1(\alpha) = & 3628800\left(15\alpha^2 + 70\alpha - 96\right), \\ \tilde{c}_2(\alpha) = & 86400\left(31\alpha^2 - 447\alpha + 5316\right), \\ \tilde{c}_3(\alpha) = & 14400\left(8\alpha^2 - 135\alpha - 1728\right), \\ \tilde{c}_4(\alpha) = & 180\left(17\alpha^2 - 442\alpha + 7740\right), \\ \tilde{c}_5(\alpha) = & 60\left(\alpha^2 + 16\alpha - 357\right), \\ \tilde{c}_6(\alpha) = & \alpha^2 - 30\alpha + 210. \end{cases}$$

- For polynomials of degree 4, $\tilde{Q}_{p,\alpha}$ is defined by

$$\tilde{Q}_{p,\alpha}(\lambda) = -\frac{\tilde{A}_{p,\alpha}(\lambda)}{120\left(169344 + h^6\lambda^3 + 84h^4\lambda^2 + 5040h^2\lambda\right)}$$

with

$$\begin{aligned}\tilde{A}_{p,\alpha}(\lambda) = \quad & \lambda^4 h^8(\alpha - 24) + 12\lambda^3 h^6(4\alpha + 287) + 1008\lambda^2 h^4(3\alpha - 305) \\ & +20160\lambda h^2(8\alpha - 165) + 5080320(\alpha - 1)\end{aligned}$$

And we have

$$Q_{p,\alpha}(\lambda) = \sum_{i=0}^{8} \lambda^i h^{2i} \tilde{c}_i(\alpha).$$

with

$$\begin{cases} \tilde{c}_0(\alpha) = & 25809651302400(\alpha - 6)^2, \\ \tilde{c}_1(\alpha) = & 204838502400\left(8\alpha^2 - 357\alpha + 1854\right), \\ \tilde{c}_2(\alpha) = & 81285120\left(698\alpha^2 + 3882\alpha + 292185\right), \\ \tilde{c}_3(\alpha) = & 203212800\left(72\alpha^2 - 13791\alpha - 328\right), \\ \tilde{c}_4(\alpha) = & 48384\left(719\alpha^2 - 12750\alpha + 2419275\right), \\ \tilde{c}_5(\alpha) = & 8064\left(76\alpha^2 - 972\alpha - 286209\right), \\ \tilde{c}_6(\alpha) = & 144\left(58\alpha^2 - 5282\alpha + 201609\right), \\ \tilde{c}_7(\alpha) = & 24\left(4\alpha^2 + 241\alpha - 6972\right), \\ \tilde{c}_8(\alpha) = & \alpha^2 - 48\alpha + 55. \end{cases}$$

- For $p = 5$, $\tilde{Q}_{p,\alpha}$ is such that

$$\tilde{Q}_{p,\alpha}(\lambda) = \frac{\tilde{A}_{p,\alpha}(\lambda)}{210\left(39916800 + \lambda^4 h^8 + 128\lambda^3 h^6 + 12960\lambda^2 h^4 + 967680\lambda h^2\right)}$$

with

$$\begin{aligned}\tilde{A}_{p,\alpha}(\lambda) = \quad & \lambda^5 h^{10}(\alpha - 35) + 70\lambda^4 h^8(\alpha + 168) + 6720\lambda^3 h^6(\alpha - 351) \\ & +302400\lambda^2 h^4(2\alpha + 385) + 8467200\lambda h^2(5\alpha - 303) + 1676505600(\alpha - 1)\end{aligned}$$

and we have

$$Q_{p,\alpha}(\lambda) = \sum_{i=0}^{10} \lambda^i h^{2i} \tilde{c}_i(\alpha)$$

with

$$\begin{cases} \tilde{c}_0(\alpha) = & 2810671026831360000\,(\alpha-15)^2\,, \\ \tilde{c}_1(\alpha) = & 28390616432640000\,(5\alpha+168)\,(\alpha-15)\,, \\ \tilde{c}_2(\alpha) = & 10241925120000\left(373\alpha^2-35067\alpha+855423\right), \\ \tilde{c}_3(\alpha) = & 3072577536000\left(24\alpha^2-895\alpha-159240\right), \\ \tilde{c}_4(\alpha) = & 1016064000\left(1151\alpha^2-11360\alpha+24379995\right), \\ \tilde{c}_5(\alpha) = & 67737600\left(257\alpha^2-3570\alpha-9096540\right), \\ \tilde{c}_6(\alpha) = & 2822400\left(76\alpha^2-2417\alpha+2988895\right), \\ \tilde{c}_7(\alpha) = & 67200\left(32\alpha^2+2383\alpha-974820\right), \\ \tilde{c}_8(\alpha) = & 140\left(131\alpha^2-37062\alpha+2285235\right), \\ \tilde{c}_9(\alpha) = & 140\left(\alpha^2+151\alpha-5912\right), \\ \tilde{c}_{10}(\alpha) = & \alpha^2-70\alpha+1190. \end{cases}$$

Contents

References

[1] C. Agut and J. Diaz. Stability analysis of the interior penalty discontinuous galerkin method for the wave equation. *INRIA Research Report*, 2010.

[2] M. Ainsworth, P. Monk, and W. Muniz. Dispersive and dissipative properties of discontinuous galerkin finite element methods for the second-order wave equation. *Journal of Scientific Computing*, 27, 2006.

[3] D. N. Arnold, F. Brezzi, B. Cockburn, and L.D. Marini. Unified analysis of disconitnuous galerkin methods for elliptic problems. *SIAM J. Numer. Anal.*, 39:1749–1779, 2002.

[4] F. Bassi and S. Rebay. A high-order accurate discontinuous finite element method for the numerical solution of the compressible navier-stokes equations. *J. Comput. Phys.*, 131:267–279, 1997.

[5] M. J. Grote, A. Schneebeli, and D. Schötzau. Dicontinuous galerkin finite element method for the wave equation. *SIAM J. on Numerical Analysis*, 44:2408–2431, 2006.

[6] M. J. Grote and D. Schötzau. Convergence analysis of a fully discrete dicontinuous galerkin method for the wave equation. *Preprint No. 2008-04*, 2008.

[7] K. Shahbazi. An explicit expression for the penalty parameter of the interior penalty method. *J. of Computational Physics*, 205:401–407, 2005.

Centre de recherche INRIA Bordeaux – Sud Ouest
Domaine Universitaire - 351, cours de la Libération - 33405 Talence Cedex (France)

Centre de recherche INRIA Grenoble – Rhône-Alpes : 655, avenue de l'Europe - 38334 Montbonnot Saint-Ismier
Centre de recherche INRIA Lille – Nord Europe : Parc Scientifique de la Haute Borne - 40, avenue Halley - 59650 Villeneuve d'Ascq
Centre de recherche INRIA Nancy – Grand Est : LORIA, Technopôle de Nancy-Brabois - Campus scientifique
615, rue du Jardin Botanique - BP 101 - 54602 Villers-lès-Nancy Cedex
Centre de recherche INRIA Paris – Rocquencourt : Domaine de Voluceau - Rocquencourt - BP 105 - 78153 Le Chesnay Cedex
Centre de recherche INRIA Rennes – Bretagne Atlantique : IRISA, Campus universitaire de Beaulieu - 35042 Rennes Cedex
Centre de recherche INRIA Saclay – Île-de-France : Parc Orsay Université - ZAC des Vignes : 4, rue Jacques Monod - 91893 Orsay Cedex
Centre de recherche INRIA Sophia Antipolis – Méditerranée : 2004, route des Lucioles - BP 93 - 06902 Sophia Antipolis Cedex

Éditeur
INRIA - Domaine de Voluceau - Rocquencourt, BP 105 - 78153 Le Chesnay Cedex (France)
http://www.inria.fr
ISSN 0249-6399